Faulting within the Mount St. Helens conduit and implications for volcanic earthquakes

John S. Pallister[1,†], Katharine V. Cashman[2], Jonathan T. Hagstrum[3], Nicholas M. Beeler[1], Seth C. Moran[1], and Roger P. Denlinger[1]

[1]*Volcano Disaster Assistance Program, U.S. Geological Survey Cascades Volcano Observatory, Vancouver, Washington 99683, USA*
[2]*Department of Geological Science, University of Oregon, Eugene, Oregon 97403, USA*
[3]*U.S. Geological Survey, MS 937, Menlo Park, California 94025, USA*

ABSTRACT

The 2004–2008 eruption of Mount St. Helens produced seven dacite spines mantled by cataclastic fault rocks, comprising an outer fault core and an inner damage zone. These fault rocks provide remarkable insights into the mechanical processes that accompany extrusion of degassed magma, insights that are useful in forecasting dome-forming eruptions. The outermost part of the fault core consists of finely comminuted fault gouge that is host to 1- to 3-mm-thick layers of extremely fine-grained slickenside-bearing ultracataclasite. Interior to the fault core, there is an ~2-m-thick damage zone composed of cataclastic breccia and sheared dacite, and interior to the damage zone, there is massive to flow-banded dacite lava of the spine interior. Structures and microtextures indicate entirely brittle deformation, including rock breakage, tensional dilation, shearing, grain flow, and microfaulting, as well as gas and fluid migration through intergranular pores and fractures in the damage zone. Slickenside lineations and consistent orientations of Riedel shears indicate upward shear of the extruding spines against adjacent conduit wall rocks.

Paleomagnetic directions, demagnetization paths, oxide mineralogy, and petrology indicate that cataclasis took place within dacite in a solidified steeply dipping volcanic conduit at temperatures above 500 °C. Low water content of matrix glass is consistent with brittle behavior at these relatively high temperatures, and the presence of tridymite indicates solidification depths of <1 km. Cataclasis was coincident with the eruption's seismogenic zone at <1.5 km.

More than a million small and low-frequency "drumbeat" earthquakes with coda magnitudes (M_d) <2.0 and frequencies <5 Hz occurred during the 2004–2008 eruption. Our field data provide a means with which to estimate slip-patch dimensions for shear planes and to compare these with estimates of slip patches based on seismic moments and shear moduli for dacite rock and granular fault gouge. Based on these comparisons, we find that aseismic creep is achieved by micron-scale displacements on Riedel shears and by granular flow, whereas the drumbeat earthquakes require millimeter to centimeter displacements on relatively large (e.g., ~1000 m^2) slip patches, possibly along observed extensive principal shear zones within the fault core but probably not along the smaller Riedel shears. Although our field and structural data are compatible with stick-slip models, they do not rule out seismic and infrasound models that call on resonance of steam-filled fractures to generate the drumbeat earthquakes. We suggest that stick-slip and gas release processes may be coupled, and that regardless of the source mechanism, the distinctive drumbeat earthquakes are proving to be an effective precursor for dome-forming eruptions.

Our data document a continuous cycle of deformation along the conduit margins beginning with episodes of fracture in the damage zone and followed by transfer of motion to the fault core. We illustrate the cycle of deformation using a hypothetical cross section of the Mount St. Helens conduit, extending from the surface to the depth of magmatic solidification.

INTRODUCTION

Understanding magma transport from crustal reservoirs to the surface and relating specific magma transport and eruptive processes to seismic signals are among the most important goals of modern volcanology—goals with profound implications for hazard analysis and eruption forecasting. Considerable progress toward these goals has been made during the past two decades (Cashman, 2004; Chouet, 1996; Kerr, 2003; McNutt, 1996, 2005; Rutherford, 2008; White, 1996; White et al., 1998). However, it is extremely rare for the magmatic conduit margins and source area for monitored volcanic earthquakes to be preserved and exposed at the surface for direct study, as is currently the case at Mount St. Helens. Here, it has been possible to directly examine rocks produced by eruption-related faulting during one of the most intensively monitored eruptions on Earth.

During the period 2004–2008, Mount St. Helens erupted seven dacite spines. Each was extruded from a vent at the south margin of the 1980–1986 lava dome, and each brought the faulted conduit margin to the surface, which was formed in the preceding days to months (Scott et al., 2008). The third, fourth, and fifth spines were recumbent "whalebacks" with smooth fault-gouge–covered upper and lateral surfaces (Fig. 1). Over a period of weeks to months, each of the spines broke into slabs and then decrepitated to varying degrees (Fig. 2). The sixth and seventh spines were erupted at steep angles and decrepitated more rapidly; however, similar fault zones mantled them while near the vent during their initial stages of extrusion, and in one exceptional case, shear concentration produced a thin layer of pseudotachylyte or sintered gouge at the margin of spine 7 (Friedlander et al., 2010). As reviewed by Cashman et al. (2008), similarities between the Mount St. Helens gouge zone and tectonic fault zones are remarkable. Both display thin slip planes composed of pulverized rock with indicators of high strain housed in 1–2-m-thick layers of granular fault gouge and bordered by several meters of cataclasite and sheared dacite. This fault-zone architecture is taken as evidence of strain-weakening behavior, with shear localization into narrow zones that act as the primary slip surfaces (e.g., Ben-Zion and Sammis, 2003).

[†]E-mail: jpallist@usgs.gov

GSA Bulletin; March/April 2013; v. 125; no. 3/4; p. 359–376; doi: 10.1130/B30716.1; 15 figures; 2 tables.

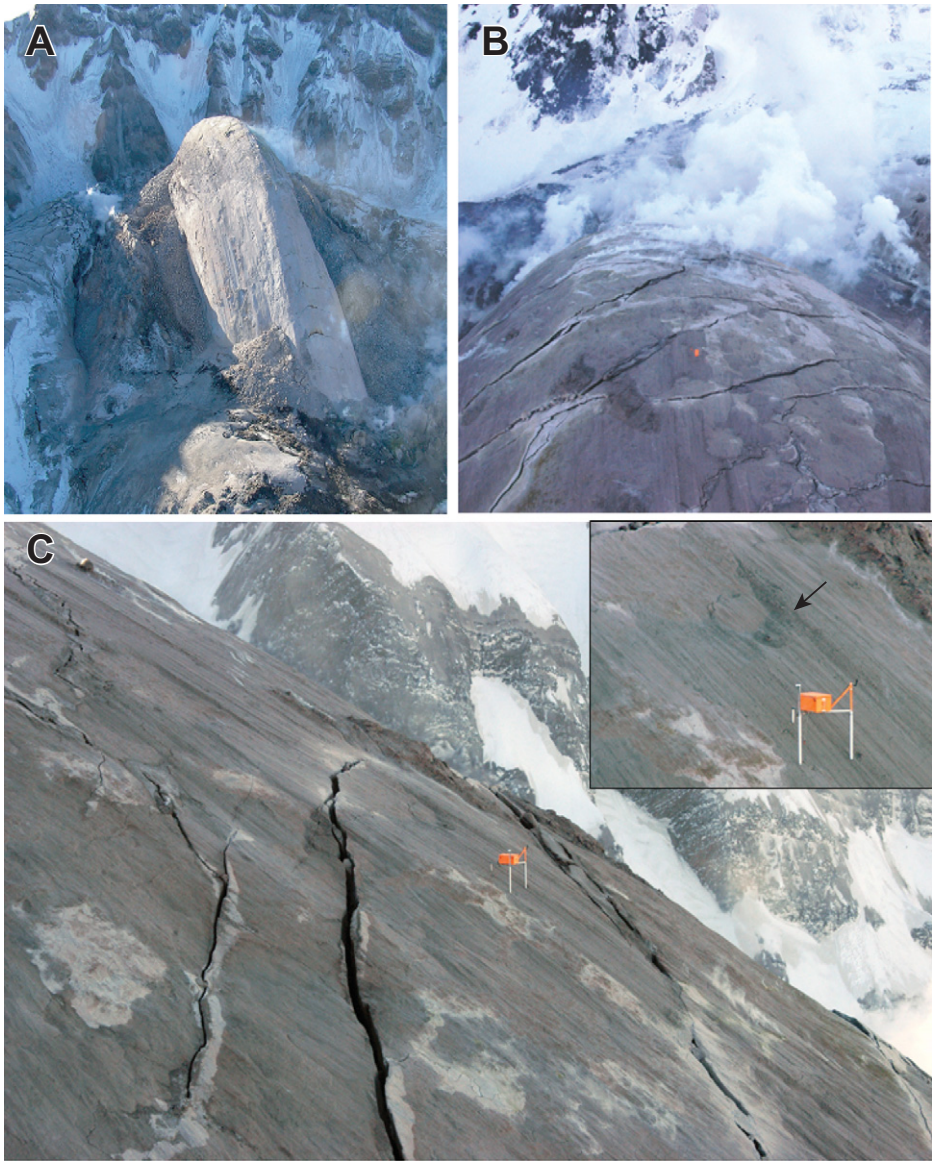

Figure 1. Photographs of spine 4 taken on 22 February (A) and 14 January 2005 (B, C). (A) View to south. (B) View looking down and to the north from above the summit of the spine. (C) View to west across spine surface showing continuity of individual slickenside lineations (grooves) over tens to hundreds of meters. The orange device at center-frame is a portable "spider" (McChesney et al., 2008), a global positioning system and seismic instrument package that was positioned by helicopter on the dome surface. The spider instrument box is 0.7 m in length. Inset image is an enlargement of the area of C near the spider, showing an eroded surface (arrow) and multiple levels of slickensided gouge. Width of the spine in A is approximately 120 m.

An extensive database of seismic and other geophysical monitoring information exists for the 2004–2008 eruption. These data were described and relationships between monitoring data and eruptive processes were published in a U.S. Geological Survey Professional Paper (Sherrod et al., 2008). One of the most unusual and distinctive features of the eruption was the occurrence of swarms of repetitive small low-frequency earthquakes with such regular repeat intervals (e.g., of about a minute), to be termed "drumbeats" (Moran et al., 2008; Waite et al., 2008). These drumbeat earthquakes have been modeled physically as the result of periodic stick-slip motion along the margins of the conduit (and their low-frequency components have been attributed to low rupture velocities and path effects; Harrington and Brodsky, 2007). A key requirement of the stick-slip models is rate-weakening behavior—a property of the gouge demonstrated in laboratory experiments (Moore et al., 2008) and necessary for the stick-slip model. Alternatively, the source of the drumbeats has been modeled seismically as the result of resonance of a steam-filled crack at shallow levels below the crater floor (Matoza et al., 2009; Waite et al., 2008). In this paper, we describe field relations and rock textures that we attribute to shearing, to stick-slip motion, fault creep, and gas migration, and we discuss how these field data help to constrain the seismogenic and physical models.

Due to the nonexplosive mode of eruption since 2006, it was possible to gain access to spines in the southeast crater area by helicopter and to conduct several days of ground-based field work during 2006–2008, while large slabs of the spines were still intact (Fig. 2). Previous work on the spine dacite and its cataclastic margin during 2004–2005 was based principally on samples collected by helicopter-assisted dredging (heli-dredging) and on field observations from a hovering helicopter (Cashman et al., 2008; Pallister et al., 2008). This is the first study of field data and oriented samples collected in situ, and it serves as the geologic framework for detailed structural and seismological studies of the fault zone (Friedlander et al., 2010; Gaunt et al., 2011; Harrington and Brodsky, 2007; Harrington and Kwiatek, 2011; Iverson, 2008; Iverson et al., 2006; Kennedy et al., 2009; Matoza et al., 2009; Moore et al., 2008; Sammonds et al., 2010; Smith et al., 2009, 2011; Waite et al., 2008). Our initial helicopter observations suggested that the spine margins were composed of 1–2-m-thick cataclasite, and textures of heli-dredge samples indicated brittle deformation. Our current work confirms and expands these interpretations with additional field observations and with textural, geochemical, and paleomagnetic data of oriented samples. Because similar whaleback spines with faulted margins have been described during other dome-forming eruptions, e.g., Montserrat (Sparks, 2000; Watts et al., 2002), Bezymianny (Bogoyavlenskaya and Kirsanov, 1981), Mount Pelee (Lacroix, 1904), and Showa-Shinzan (Mimatsu, 1995), we believe that our results may be broadly applicable to other dome-forming eruptions.

FIELD RELATIONS AND STRATIGRAPHIC SAMPLING

In contrast to the episodic 1980–1986 dome-forming eruptions at Mount St. Helens, which erupted mainly viscous lava flow lobes (Swanson and Holcomb, 1990), the 2004–2008 eruption of Mount St. Helens erupted exclusively

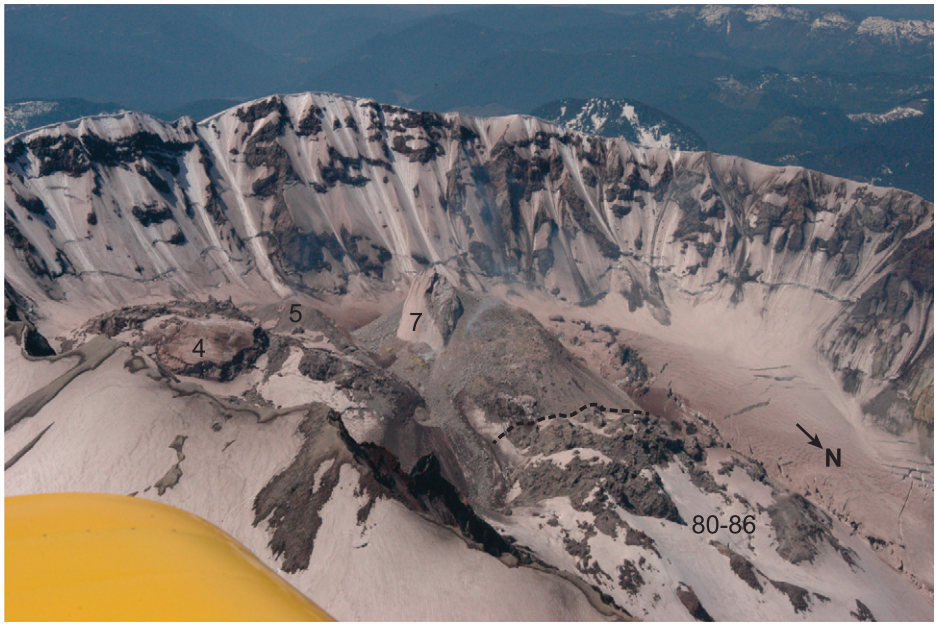

Figure 2. Oblique aerial photograph of Mount St. Helens crater on 17 May 2006, looking southwest and showing remnants of spines 4 and 5 in southeast sector of crater (4, 5) and decrepitating mound of debris surrounding spine 7, which is rising steeply from vent. Note the fume rising from the vent area at the north margin of spine 7. The 1980–1986 dome (80–86) is the lower mass of rock with snow cover north of spine 7. Dashed line indicates contact between the 1980–1986 and 2004–2008 domes. Pink to gray ash on snow is from small ash clouds generated during repeated collapses of spine 7. Diameter of the Mount St. Helens crater is approximately 2 km.

solidified dacite (Vallance et al., 2008). Solidification took place within the upper kilometer below the vent, such that no lava flowage occurred at the surface (Fig. 3). Instead, inclined whaleback spines (numbered 1–5), and then subvertical spines (6, 7) were extruded. As documented in photogeologic maps (Herriott et al., 2008), the first three spines had remarkably continuous striated upper surfaces that dipped 30°–60° back toward and into the vent (to the northwest). The third and fourth spines plowed southeast across the crater floor, uplifting and dividing the Crater Glacier (Vallance et al., 2008; Walder et al., 2008). Upon reaching the southeast crater wall, the third spine fractured and was abandoned as a fourth spine was extruded, overriding the west margin of the third spine and shifting the axis of extrusion to the south. When spine 4 reached the south crater wall in January and February 2005, an axial fault zone formed along its crest, and the direction of extrusion at the vent shifted slightly west as spine 5 began to emerge. Once abandoned by the vent, spine 4 broke up, with collapse of an axial graben block down and to the west. The eastern margin was buttressed by the earlier erupted spine 3. A vertical shear zone also developed within spine 5 as it was abandoned (in July–August 2005). Development of this shear zone coincided with a shift to higher-frequency earthquakes located in the immediate vicinity of the shear zone (Moran et al., 2008; Vallance et al., 2008). This relationship confirms the very shallow locations of earthquakes (Thelen et al., 2008) and that they postdate solidification of the spines. The sixth and seventh spines were also buttressed by previous spines, rose more steeply from the vent, decrepitated in place, and produced mounds of blocks and boulders in the southwest part of the crater. This latter process eventually buried the vent in rubble and resulted in endogenous dome growth—a mode of eruption that continued to the end of the eruption in January 2008.

By 2008, outcrops of the fourth spine were exposed over an area of ~200 m by 400 m in the southeast crater. The exposures included an intact remnant of the whaleback surface of spine 4 with dimensions of ~100 m by 200 m on the eastern side of its axial graben. The walls of the graben exposed vertical sections through the spine margin, which extended several tens of meters into the interior of the spine. We focused our field work in these areas.

Figure 4 shows a representative section showing commonly observed structures in sections through the fault rocks comprising the outer margin of spine 4. From the outer surface to the interior, the spine margin consists of: (1) finely comminuted sandy to powdery fault gouge (0–2 m thick), typically containing one or more thin surface-parallel layers (1–3 mm thick) of slickenside-striated ultracataclasite, (2) cataclastic breccia (~1 m thick), cut by prominent Riedel fractures, (3) sheared dacite (typically 1–2 m thick), also cut by Riedel shears, and (4) intact dacite, which is massive or locally flow banded and presumably extends to a similar sequence of fault rocks at the opposite side of the spine.

The gouge varies in thickness from spine to spine, ranging from a few centimeters to ~2 m. Soft fault gouge at least 30 cm thick was observed and sampled on spine 3 within hours of eruption, and photographs of the surface of spine 4 taken from a helicopter shortly after eruption suggest that the gouge locally exceeded a meter in thickness, a relationship confirmed by our field work. Upon eruption, thin ultracataclasite layers at the surface of and within sandy gouge covered most of the surfaces of the spines. These surface and near-surface layers are characterized by well-developed slickensides on 1–3-mm-thick layers of extremely fine-grained ultracataclasite (<5 μm grain size). Slickenside lineations are parallel to the eruption-transport direction and extend for many tens of meters in the direction of extrusion (Fig. 1). In detail, slickenside fan structures have individual fan- or cone-shaped distributions (Fig. 5), which individually cover areas of less than a few tens of square centimeters. Asperities on slickenside surfaces suggest both upward and downward motion of the spine with respect to bounding rocks, perhaps representing either an increase in gas pressure pushing the spine upward followed by depressurization and downward motion upon gas release, or oscillation of the spine above a compressible magma at greater depth. Lack of postemplacement erosion of some areas of the surface layer of spine 4 was demonstrated by discovery of orange paint fragments adhering to the surface of ultracataclasite layers near the southern terminus of spine 4. The paint was applied to the newly erupted surface near the vent during a helicopter-borne paint-bombing mission on 14 January 2005 to help in measuring extrusion velocity. It rode on the back of the spine during transport south across the crater floor. This discovery dates the outcrops in our study area to middle to late January 2005. In addition, the preservation of paint on this locally thin section of gouge shows that not all of the observed variation in thickness of the outer powdery gouge is the result of posteruption surficial erosion; variation in thickness also resulted from processes that took place below vent level. Confirmation of variable

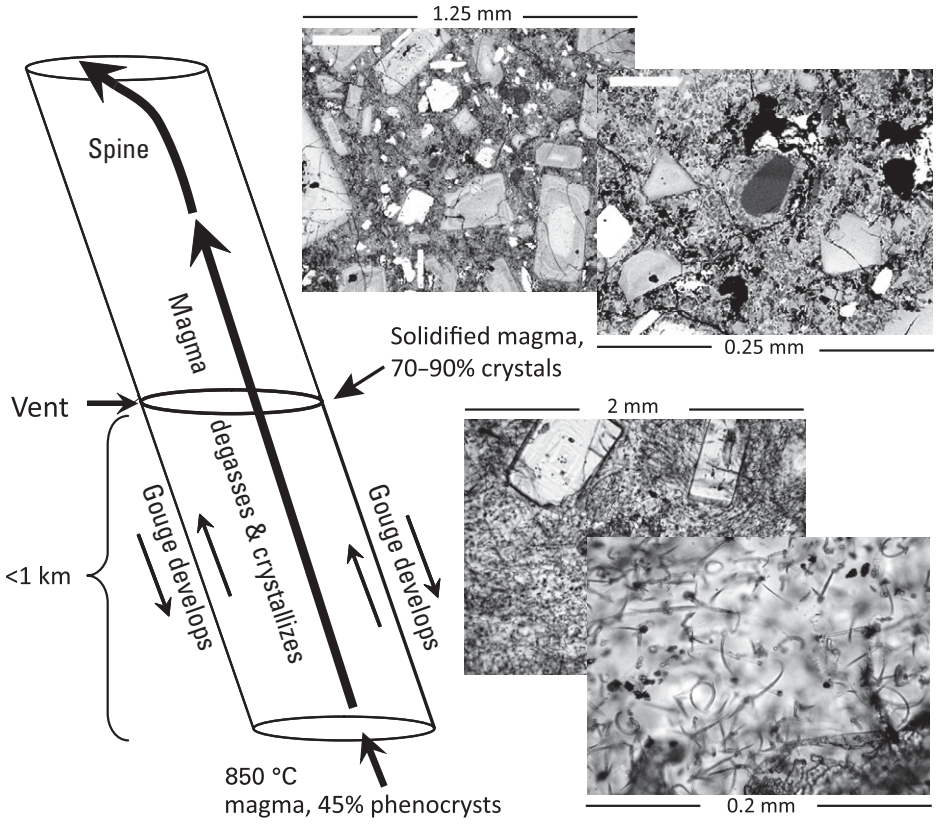

Figure 3. Diagram illustrating growth and solidification of dacite of spine 4 with development of gouge along the margins due to shear couple between the rising dacite and wall rocks. Photomicrographs are from samples dredged during the eruption and illustrate the effects of decompression crystallization of groundmass melt during ascent through the upper 1 km of the conduit (Pallister et al., 2008). The lower two images are from an unusual glassy sample that was dredged from an early phase of spine 1. The curvilinear needles are rapidly grown pyroxene. The upper photomicrographs are from a typical sample of the interior of spine 4, showing the extensive crystallization of the groundmass, which resulted in solidification.

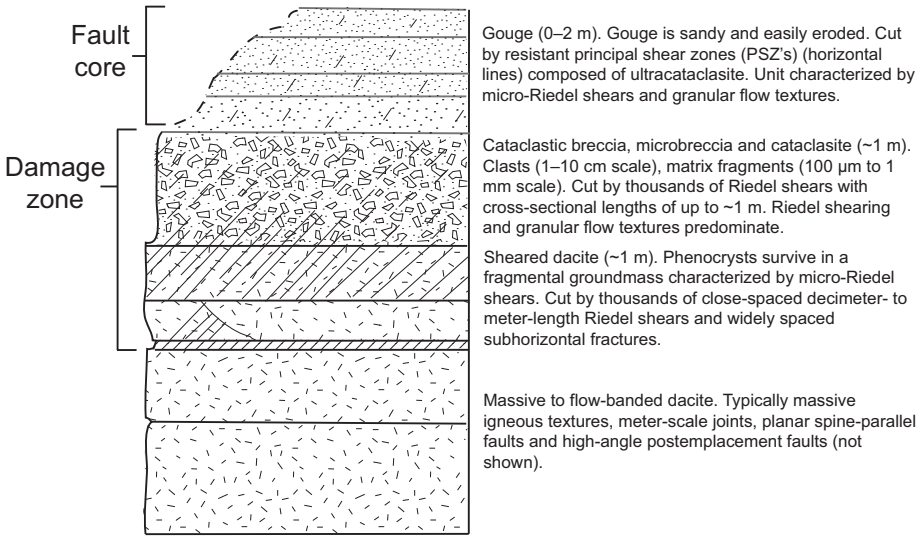

Figure 4. Composite cross section of the faulted margin of spine 4. The fault zone varies from location to location, from <1 m to as much as ~4 m in composite thickness.

gouge thickness is provided by outcrops on the east flank of spine 4, where more than a meter of poorly consolidated gouge is preserved in a local downdropped fault block. In this outcrop, multiple resistant, millimeter-thickness ultracataclasite layers are preserved within the soft gouge (Fig. 6), and the innermost of these ultracataclasite layers is stratigraphically equivalent to the outer surface of the more eroded exposures outside the area of the downdropped block.

The cataclastic breccia below the soft gouge is characterized by a fragmental character and by development of thin shear zones, which occur at angles of 20°–40° relative to the spine margin and ultracataclasite layers (Fig. 7). These relatively high-angle shears are even more prominent in the underlying sheared dacite (Fig. 8). By analogy to similar shear structures described in brittle deformation experiments and strike-slip fault zones (Ahlgren, 2001; Moore and Byerlee, 1991; Riedel, 1929; Skempton, 1966; Tchalenko, 1970), we interpret these structures as Riedel shears. Following the tectonic fault literature, the through-going ultracataclasite fault layers within the gouge are designated as principal shear zones (Skempton, 1966). Riedel shears occur at cross-sectional lengths ranging from 1 to 2 m in the damage zones to microns in the fault core gouge. The maximum lateral extents of the Riedel shears are difficult to measure because many of them merge into principal shear zones, which range from meters to tens of meters in lateral extent (Fig. 9). Clasts in the cataclastic breccia vary widely in diameter, ranging from decimeter to submillimeter scales. In some outcrops, there is a gradational contact between the breccia and the gouge in which the clast size of the breccia decreases continuously to the microscopic scale observed in the gouge. In other outcrops, cataclastic breccia and gouge are separated abruptly by a spine-surface–parallel principal shear zone.

Interior to the cataclastic breccias, there is sheared dacite, cut by prominent Riedel shears. Deformation in the sheared dacite is partitioned mainly into the groundmass. By extrapolating from the average density of such megascopic shears in outcrops (i.e., 10–100 per linear meter of spine) to the total extruded length of spines (3–5 km, assuming an average rate of 3–4 m d^{-1} for 3 yr; Major et al., 2008), we estimate that there are hundreds of thousands of decimeter- to meter-scale Riedel shears cutting the cataclastic breccia and the sheared dacite of the spines. We consider such an extrapolation to be reasonable, given a similar density of megascopic Riedel shears observed during heli-dredge sampling of the spines over the course of the eruption (Pallister et al., 2008).

Interior to the sheared dacite, there is massive to flow-banded dacite with irregular to weak columnar jointing. Flow foliation is locally exposed at distances of 10–20 m into the interior of spine 4, although in most outcrops, the interior dacite appears massive. Some outcrops of the cataclastic breccia display oxidized iron staining along shears (Fig. 7), indicating transport of gas or hydrothermal fluids along these fractures.

CHEMICAL COMPOSITIONS OF CATACLASITE

The chemical compositions and petrology of intact dacite from the 2004–2008 eruption were detailed in a series of papers included in the U.S. Geological Survey Professional Paper on the eruption (e.g., Pallister et al., 2008; Rutherford and Devine, 2008; Blundy et al., 2008; and others). Here, we review only compositional and mineralogic features of the cataclastic rocks.

Samples of gouge were collected by heli-dredging of spine surfaces seven times during the first 2 yr of the eruption. Five of the samples have major-element compositions that overlap with those of the dacite, but one sample is distinctly more mafic (Table 1). The mafic gouge sample was collected from spine 3 shortly after the eruption began in October 2004. This early sample likely reflects disruption and incorporation of mafic wall rocks into the fault zone during the initial intrusion of spine magma. A second gouge sample erupted in July 2005 has slightly low SiO_2 and K_2O and high Al_2O_3 and CaO. This sample represents a time when spine 5 was breaking up and spine 6 was beginning to emerge.

Wall rocks to the conduit at depths greater than ~100–200 m (approximate thickness of 1980 deposits in this part of the crater) are mainly basaltic andesites of the Castle Creek period (Clynne et al., 2008). Projection of contacts from the crater mouth suggests that these rocks are host for the conduit over a vertical thickness of at least 100 m. Consequently, the mafic gouge composition suggests that spine-boundary faulting extended from dacite of the conduit into these more mafic wall rocks. This hypothesis was confirmed during field work in 2008, when we found Castle Creek–type basaltic andesite lava clasts in the outermost exposures of thick gouge atop spine 4.

MINERALOGY

Most of the cataclasites of the spine margins were derived from rock with an identical mineral assemblage to that of the host dacite. Breccia clasts are crystal rich, with phenocrysts of plagioclase, hypersthene, amphibole, and Fe-Ti oxides, and all have microcrystalline groundmasses. Microlites include hypersthene, plagioclase, oxides, tridymite, and cristobalite. Virtually all the groundmass glass in the clasts has crystallized to an extremely fine-grained mosaic of microlites. These samples are similar to heli-dredged samples from many other exposures of the spines, as described by Pallister et al. (2008) and Cashman et al. (2008). Samples from the spine margins show marked evidence of vapor transport and deposition. At microscopic scales, fractures and pore spaces are lined with vapor-phase minerals. The vapor-phase assemblage consists mainly of microlites of Na- and K-rich plagioclase, cristobalite, and iron oxides (see figs. 7 and 8 *in* Pallister et al., 2008). The degree of vapor-phase crystallization and infilling of the groundmasses increased with time and contributed to increased rock strength through the sequence of spine eruptions (Pallister et al., 2008; Smith et al., 2011).

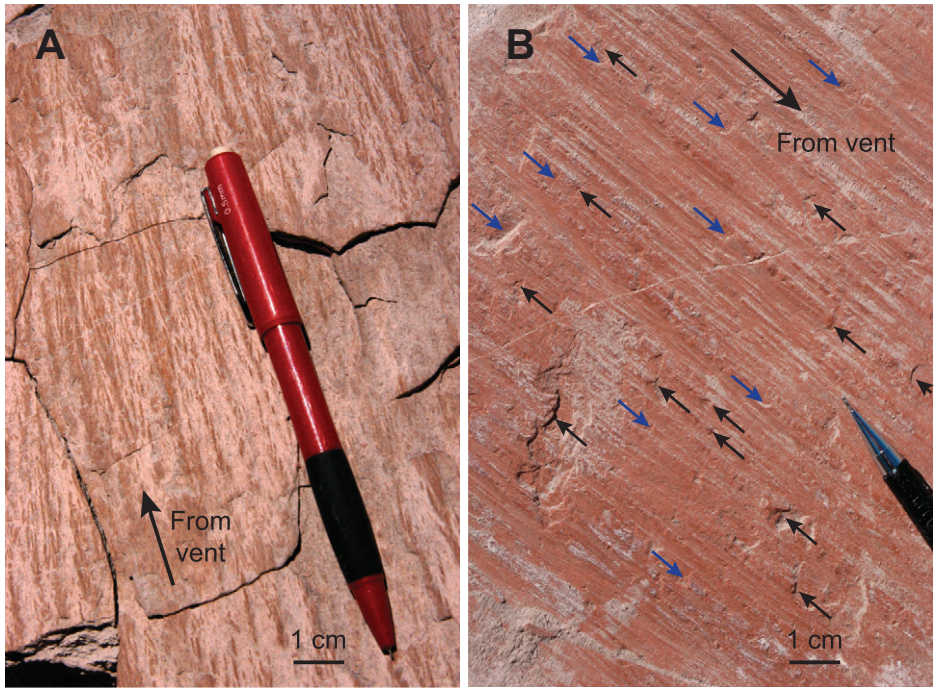

Figure 5. Surfaces of spines showing development of slickenside fans on the surface of spine 4 (A) and along a shear zone in spine 5 (B). Arrows label directions from the vent in both images. Asperities, which are sometimes used as fault-movement indicators (Doblas, 1998), are evident in B. Small arrows indicate apparent movements of this surface that are both up (from vent) and down relative to formerly adjacent wall rocks.

MICROTEXTURES

Our examination of thin sections from several dozen spine samples collected by heli-dredging and in situ sampling from spine 4 shows that undeformed dacite with magmatic textures is present at depths of 1–5 m into the spine and that the degree of shearing and granulation increases from the interior outward. A suite of oriented samples was collected from the wall of an open fracture through the margin of spine 4. These samples span a distance of ~5 m from the fault core at the spine surface into intact dacite of the spine interior. The gouge zone of the fault core at this locality is relatively thin (only ~5 cm). Examination of samples in thin section and scanning electron microscopy (SEM) images (Fig. 10) show that the fault rocks display an extremely wide range in degree of deformation and grain size, spanning more than four orders of magnitude in fragment diameter (from >1 cm to <1 μm). The same wide range was seen in heli-dredged samples (Cashman et al., 2008).

From interior to exterior of the spine, brittle deformation is first observed in the groundmass of the sheared dacite at a depth of 1–2 m into the damage zone, where shearing is concentrated in the groundmass, leaving phenocrysts largely intact (Figs. 10E and 11). In this zone, shearing produced a prominent set of conjugate micro-Riedel shears, which divert around the phenocrysts. This indicates a competence contrast between the matrix and crystals and "tearing" of the matrix to increase porosity and permeabil-

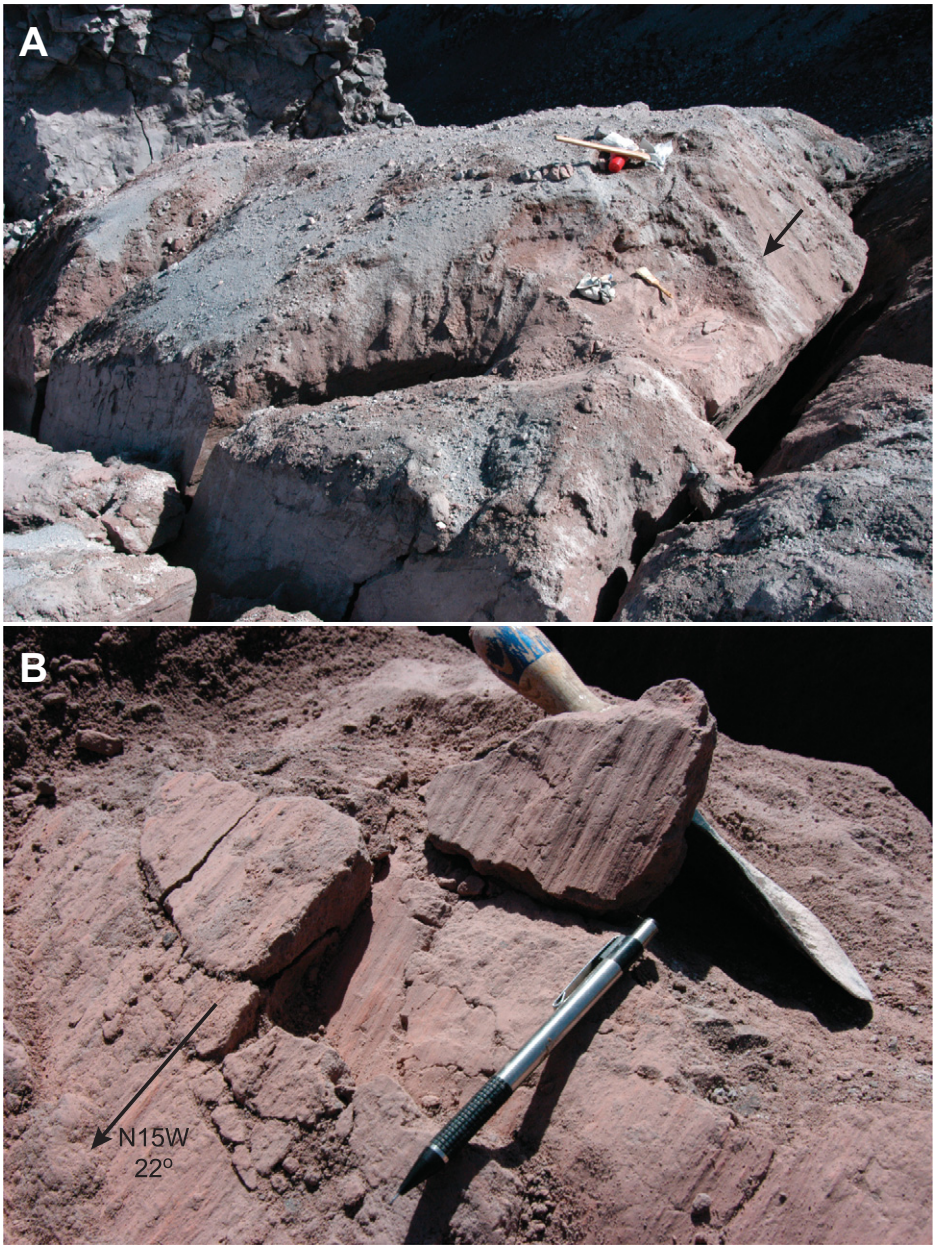

Figure 6. (A) Outcrop of soft gouge (fault core) ~2 m thick in a downdropped block of the surface of spine 4. The gouge contains several surface-parallel ultracataclasite layers as seen in the excavated area indicated by the arrow. (B) Close up photograph of two parallel slickensided ultracataclasite layers within the gouge in the excavated part of the outcrop (arrow indicates orientation of lineations; vent is also to the north-northwest).

ity. This process also provides a mechanism for ultimately generating fault gouge and demonstrates that to crush a dense rock, porosity must be generated first (Brace et al., 1966). Here, that porosity is generated by extension and shear, and then the rock is susceptible to pulverization and production of gouge.

The widest range in grain size is found in the overlying cataclastic breccia, which has clasts of variably deformed dacite that range in size from millimeter to decimeter scale and that are contained in a cataclastic matrix with fragments that range to micron scale. At a distance of 20 cm into the cataclastic breccia of the damage zone in our measured section, the matrix between centimeter-size dacite clasts consists of a seriate fabric with variably broken and rotated phenocrysts (100 μm to 2 mm) set in a cataclastic matrix with an average grain size of 10–100 μm (Fig. 10D).

In most outcrops, there is a dramatic contrast in grain size between the cataclastic breccia of the damage zone and the gouge of the fault core. This is evident in Figures 10A, 10B, and 10C, in which the grain size of the gouge ranges from ~1 mm to 1 μm. Such a reduction in grain size involved not just shearing but abrasion, grain rotation, granular flow, and alignment of groundmass fragments. With continued deformation, shearing was transferred into ultracataclasite layers, characterized by extreme grain-size reduction and average grain sizes of <5 μm in these 1–3-mm-thick shear layers. Alignment of grains into thin bands in the ultracataclasite layers resulted from shearing and sliding of grains and grain-aggregate lenses past one another. Relict phenocrysts adjacent to the ultracataclasite layers were rolled or shattered (Fig. 10B). Micro-Riedel fractures (Fig. 10A) within these sublayers have similar orientations to their macroscopic cousins, indicating that the same mode of shear deformation seen in the cataclastic breccia and sheared dacite extended into the gouge layer. Within the gouge, dacite fragments that are large enough to be characterized with the SEM are nearly holocrystalline (relict glass contents are typically <10%), consistent with complete solidification of the ascending magma before cataclasis. We found no evidence of shear melting and production of pseudotachylyte in spine 4; however, pseudotachylyte- or sintered-gouge–lined shears have recently been found in the margin of spine 7 by Friedlander et al. (2010).

PALEOMAGNETISM

Specimens for paleomagnetic analysis were drilled in the laboratory from three oriented samples of the cataclastic breccia zone from spine 4. The cores contained multiple fragments and matrix with varying degrees of shear fragmentation and grain rotation. The specimens were subjected to either progressive alternating field or thermal demagnetization up to 90 mT and 570 °C, respectively (Fig. 12). Both methods produced univectorial decay of the thermo-remnant magnetization acquired during cooling of the cataclasite below the Curie temperature of its constituent magnetic minerals. Least-squares lines (Kirschvink, 1980) were fitted to the demagnetization steps, and the sample means were calculated using standard methods (Fisher, 1953).

Paleomagnetic directions for the cataclasite have northerly declinations and shallow inclinations (Fig. 12), consistent with observations that spine 4 emerged from the vent at an angle of 40° to 50° and then rotated about a WSW-ENE fold axis to a subhorizontal position as it

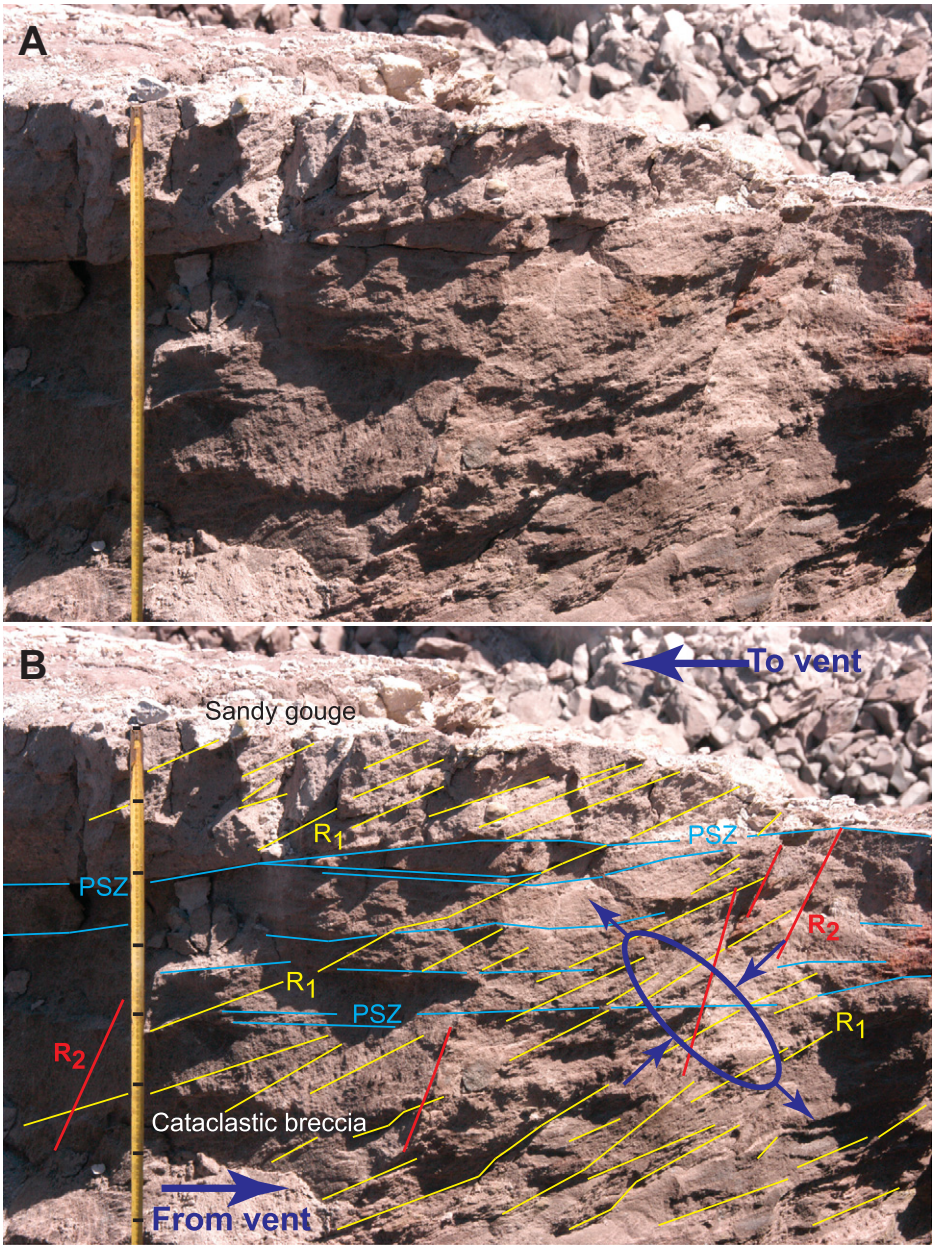

Figure 7. Natural cross sections through the fault core showing: (A) Cataclastic breccia cut by dozens of Riedel shears and overlain by soft powdery gouge. Vertical ruler is 73 cm high in frame. (B) Same image with labels for prominent Riedel shears (R1, synthetic shears; R2, antithetic shears), through-going principal shear zones (PSZ), where arrows indicate directions toward and away from vent, as well as shear couple between solidified dacite and wall rocks, and interpreted strain ellipsoid for the sense of shear dislocation in the outcrop.

moved across the crater floor to the SSE. The demagnetization data indicate that the predominant magnetic mineral carrying the remanent magnetization is titanomagnetite and that ~70% of the magnetization was unblocked and thus likely acquired between 400 °C and 570 °C. These data also show that the outer carapace of the spine most likely cooled below 570 °C before rotation onto the crater floor, consistent with Forward-Looking Infrared Radiometer measurements of <200 °C for surfaces of the just-erupted spines (Schneider et al., 2008). More importantly, the coherence of magnetization within the cataclastic rocks demonstrates that the intense brittle deformation, grain rotation, and oxidation involved in gouge formation took place at >570 °C and while the spine was still steeply oriented within the conduit.

Fe-Ti OXIDE THERMOBAROMETRY

Fe-Ti oxide compositions, equilibrium temperatures, and oxygen fugacities for samples from the cataclasite breccia and sheared dacite are given in Table 2. Because of a good match to experimental calibrations of magmatic temperatures for Mount St. Helens dacites and to facilitate direct comparison to other determinations from Mount St. Helens (Blundy et al., 2006, 2008; Pallister et al., 2008; Rutherford and Devine, 2008), we use the Fe-Ti exchange thermobarometer of Andersen and Lindsay (1988) and the solution model of Stormer (1983).

Most of the titanomagnetites in our gouge samples have oxidation-exsolution lamella, making it difficult to obtain reliable thermobarometric results. However, one sample (P-60622-B, an ultracataclasite from the outer margin of spine 4) contained a few larger dacite fragments (0.15 mm) with unexsolved titanomagnetite grains. We analyzed three of these grain pairs. We also analyzed a typical touching grain pair as well as isolated matrix grains from the fine-grained matrix of the sample in which the titanomagnetite phases were exsolved. For these exsolved grains, we used large beam diameters to effectively average the compositions. The thermobarometric results are shown in Table 2, and average temperatures and f_{O_2} are compared to results from other Mount St. Helens samples in Figure 13. All of the grain pairs used for thermobarometry in this study have Mg/Mn ratios within error limits of the equilibrium line of Bacon and Hirschmann (1988).

Apparent temperatures of Fe-Ti oxide pairs from the cataclastic rocks range from 857 °C to 936 °C and overlap with the ranges in temperature and oxygen fugacity determined from unexsolved touching oxide grain pairs in intact dacite samples collected during the eruption (Pallister et al., 2008). Wide-ranging and anomalously high temperatures determined from the intact samples are attributed to disequilibrium heating, brought about by latent heat release during the rapid and extensive crystallization of groundmass phases in the dacite (Blundy et al., 2006; Pallister et al., 2008).

Given the well-defined demagnetization paths for oxides from the cataclasites and their locations at the spine margins, we had initially anticipated that these samples might have cooled more rapidly than the dacite of the spine interiors and therefore better recorded initial magmatic temperatures, estimated at ~850 °C (Pallister et al., 2008; Rutherford and Devine, 2008). However, the wide range in apparent temperatures and oxygen fugacities, and the extensive groundmass crystallization show that the fault rocks were affected by the same latent

heating process as the spine-interior dacite. We attribute the simple demagnetization paths for these samples to formation of small magnetic domains produced by exsolution during vapor-phase oxidation, and we conclude that all rocks of the spines were subjected to extensive decompression crystallization and solidification prior to deformation (i.e., there were no quenched margins).

DISCUSSION

Analogy to Tectonic Fault Zones

By analogy to shallow crustal fault zones (Caine et al., 1996; Chester and Logan, 1987; Sibson, 1977), the ultracataclasite gouge layer represents a "fault core," which accommodates most of the displacement, that is mantled by a thicker "damage zone," which shows a lesser degree of cataclasis (Fig. 4). The Mount St. Helens fault core and damage zone are one-sided; only the inner layers of the classic fault zone structure are exposed, and the degree of deformation increases from damage zone to fault core, consistent with progressive development and thickening of the fault core, as also seen in tectonic faults (Scholz, 1987). Presumably, outer layers of the fault zone formed in wall rocks of the conduit but remained in the subsurface beneath the vent. Based on the semicircular outcrop of the exposed sector of the vent and the extent of fault rocks, we suggest that the fault zone surrounding the Mount St. Helens conduit is roughly cylindrical (Figs. 1A and 3). However, because of the inclined orientation of the spines, only the upper half of this cylindrical fault is exposed. Also, because of the inclined orientation of shallow levels of the conduit (as inferred from the initial northward dip of the spines as they emerged from the vent), the upper half of the spines and the northern half of the conduit down to a depth of at least a hundred meters must have been under tension, doubtlessly contributing to the exquisite preservation of the fault-zone rocks. The inclination of the spines to the north is thought to be a result of the conduit having been diverted by the solidified root of the 1980–1986 dome (Vallance et al., 2008).

Structures in the damage zone document three dominant modes of brittle shear failure: small-scale and pervasive synthetic Riedel-shears, minor antithetic Riedel shears, and through-going spine-margin-parallel principal shear zones, the latter mantling the entire primary surfaces of the spines. The sheared dacite and cataclastic breccia of the damage zone contain multiple generations of Riedel shears, and crosscutting relationships, which show that the timing of Riedel shearing preceded most but overlapped with some of the dislocations on individual principal shear zones. Just as the grain size of fragments in the fault zone ranges over orders of magnitude, so do the dimensions of the Riedel shears. Visible shear-plane spacing varies from decimeters to centimeters for the prominent shears visible in outcrops to microns in thin sections.

In outcrop, Riedel shears of the damage zone are typically separated by through-going transport-parallel principal shear zones. The prominent synthetic Riedel shears are inclined 20° to 40° relative to the principal shear zones and spine boundary, and they consistently dip toward the vent. For the case of simple shear, the Coulomb failure criterion predicts that the initial Riedel shears are inclined at $\pi/4 - \phi/2$ with respect to the maximum principal stress (Skempton, 1966; ϕ is the internal angle of friction). Consequently, these inclinations suggest an internal angle of friction for the host dacite at the time of deformation of ~40°. The sense of shear is consistent with upward transport of the interior of the extruding spine relative to wall rocks (Figs. 3 and 7B).

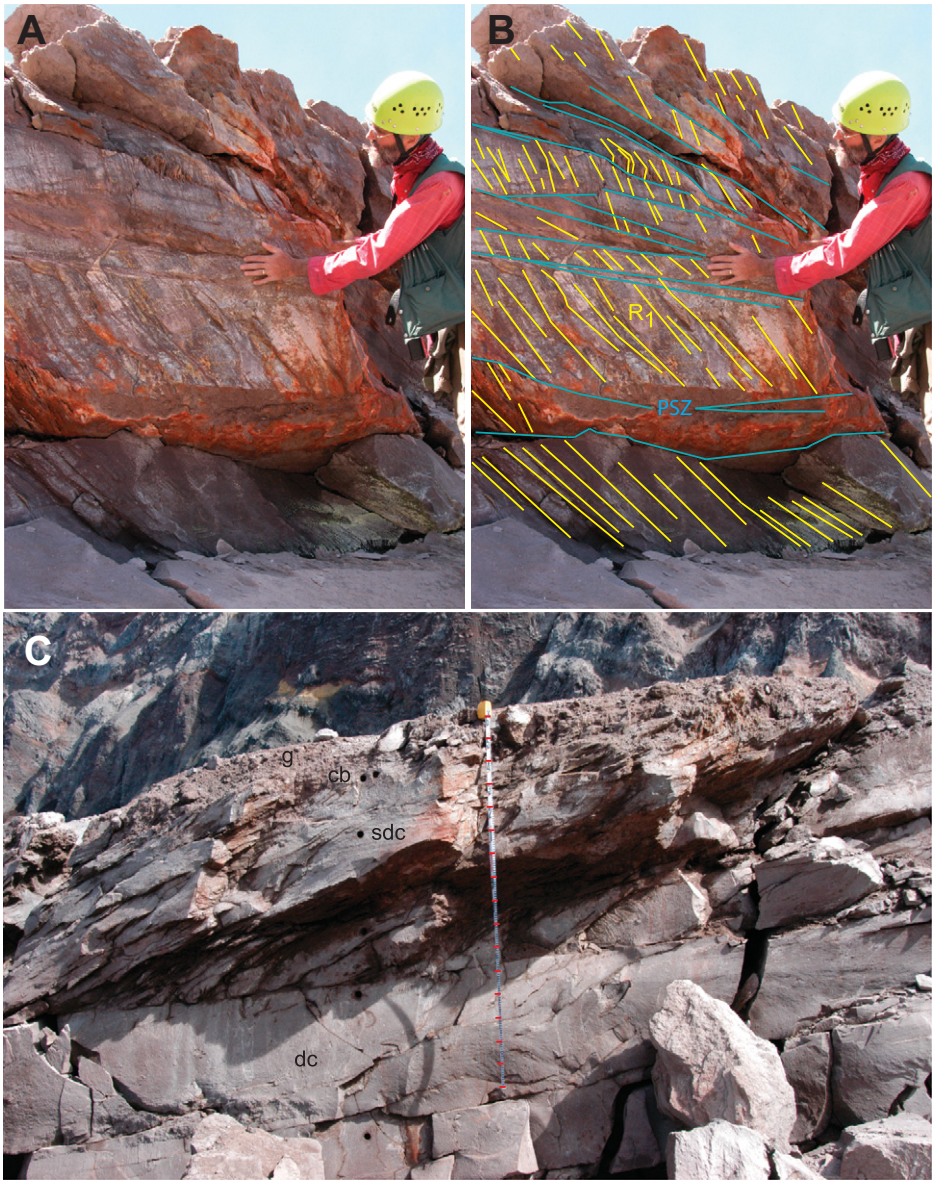

Figure 8. (A–B) Sheared dacite cut by hydrothermally altered synthetic Riedel shears (R_1) and principal shear zones (PSZ). (C) Typical cross section through the fault zone extending from massive dacite (dc) at the base of the outcrop through sheared dacite (sdc) in the central area to cataclastic breccia (cb) and gouge (g) at the surface. Tape is 1.6 m long.

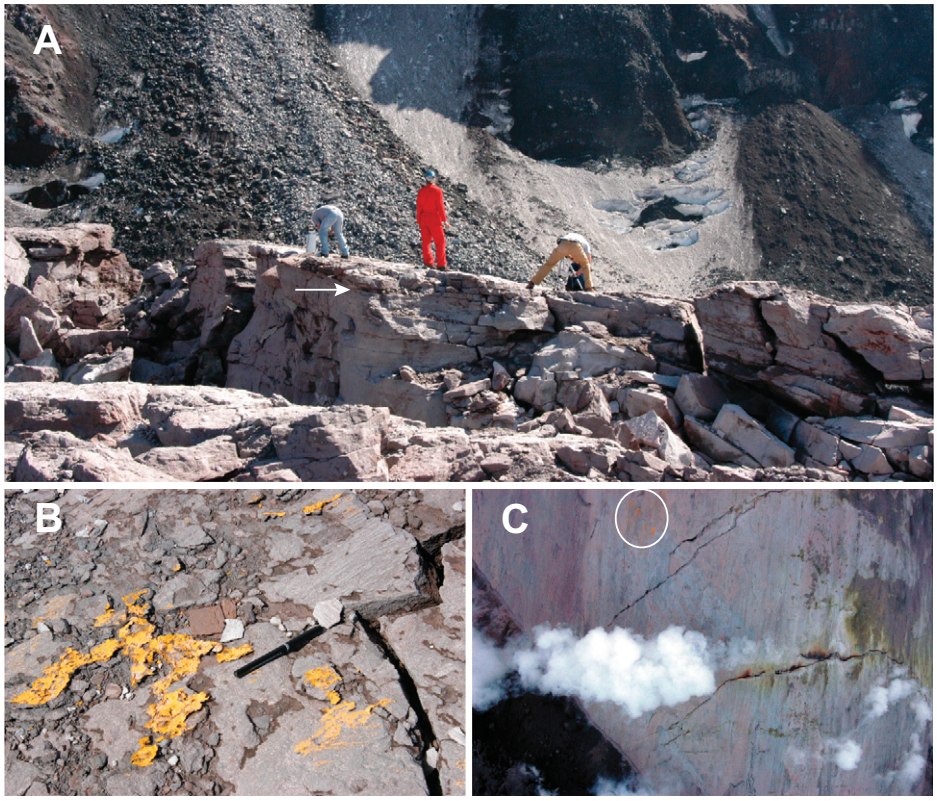

Figure 9. (A) Photograph taken on 8 August 2008 of outer part of spine 4, near its southern terminus and looking south along the spine axis. People are standing on gouge and ultracataclasite layers at the outer exposed surface of the spine with the southern crater wall in the background. Note the continuity of subhorizontal fractures (e.g., at arrow), which extend over tens of meters. Smaller Riedel shears terminate against or merge with these more areally extensive fractures. (B) Close-up of spine surface in A showing yellow paint that was applied by paint bombing to the spine surface when it was ~25 m above the vent on 14 January 2005, as shown within the circle in C. (C) A near-vertical contrast-enhanced view down at the spine as it emerged from the vent (dark material at lower left is rock debris at the vent margin; compare to Fig. 1A). Circle in C is approximately 10 m in diameter.

The presence of a relatively thick fault core located immediately outside the damage zone and containing micro-Riedel shears of similar orientation indicates development of the damage zone and the fault core as an ongoing and overlapping process that accompanied extrusion of the spines. It is apparent that the ultracataclasite layers formed as the Riedel shears intersected and became interconnected, much as observed in clay-cake experiments and shallow fault zones (Tchalenko, 1970). We interpret the increase in degree of deformation from the interior of the spine to the outermost exposed surfaces to indicate increasing fault motion from interior sheared dacite, through cataclasite, to gouge, with maximum motion partitioned into the ultracataclasite layers that comprise the fault's principal shear zone, while also recognizing that there was a continuous supply of fresh rock as the magma solidified at <1 km depth that was then sheared as it moved upward (see following; Kennedy and Russell, 2011).

Cross Section of the Conduit Margin Fault Zone

A schematic cross section through the 2004–2008 Mount St. Helens conduit is shown in Figure 14. The solidification front for the dacite magma is shown at a depth of <1 km, based on petrologic constraints, including presence of tridymite as a late groundmass phase (Cashman et al., 2008; Pallister et al., 2008). At depths below the level of the solidification front, relative motion between the conduit walls and magma was accommodated by viscous magmatic flow. Above this level and as the solidified dacite continued to rise, a shear couple formed between the solidified dacite and the wall rocks. Initial motion was accommodated by Riedel shearing within the dacite, resulting in a stress drop upon formation. With increasing relative motion, shearing, brecciation, and cataclasis reduced grain sizes and generated the fault-core gouge zone and the ultracataclasite layers.

Our SEM data (Fig. 10) show that the cataclastic rocks of the damage zone have high degrees of fracture porosity and permeability. Accordingly, we suggest that transport of gases liberated during solidification of dacite was preferentially along the margins of the conduit and powered the gas emissions and explosions that emanated from the vents at or near the upper spine margins at their point of emergence (Fig. 15; see also Rowe et al., 2008; Vallance et al., 2008). Preferential vertical transport of fluids within the damage-zone fault rocks and fault-core rocks is favored by laboratory measurements on the Mount St. Helens gouge, which show that permeability parallel to the transport direction is several orders of magnitude greater than that perpendicular to the conduit margin (Gaunt et al., 2011).

A key feature of our cross section is continuous growth of the fault zone, which resulted in repeated episodes of deformation of similar scales and in similar locations. Rising solidified dacite was deformed at the conduit margins as it passed through the system in conveyor-belt–like fashion. Although new structures were continuously forming, similarities in the relative positions and spatial dimensions of shearing and faulting were retained for prolonged periods.

Relation to Earthquakes

The coincidence of petrologically constrained final solidification depths of less than about a kilometer (Cashman et al., 2008; Pallister et al., 2008) with the depths of earthquakes (Moran et al., 2008; Thelen et al., 2008) and the presence of cataclastic rocks mantling the spines is circumstantial evidence for an association between the processes that fragmented the rocks and those that generated the earthquakes. The fact that we observe a fault core and damage zone profile (Caine et al., 1996) at the outer margin of the spines and hundreds of thousands of Riedel shears with orientations that indicate shear between an upwardly moving solidified conduit-plug and adjacent wall rocks argues for similar processes to those observed in shallow tectonic faults. We note that acoustic emissions have been recorded during experimental deformation of silica-rich magmas at high temperatures (up to 900 °C), showing that seismic fracture of even nonsolidified magma is possible (Goto,

TABLE 1. BULK-ROCK MAJOR-ELEMENT COMPOSITION OF GOUGE SAMPLES FROM MOUNT ST. HELENS SPINES COMPARED TO AVERAGE COMPOSITION OF THE 2004–2006 SPINE DACITE

Field no.:			SH303-1	SH307-2B	SH314-G	SH315-2	SH320-1	SH326-2A	SH327-1
Spine no.:	3–7		3	4	5	4	5	7	7
Estimated eruption date:	2004–2006		18 October 2004	07 February 2005	17 April 2005	01 April 2005	01 July 2005	10 January 2006	26 March 2006
	AVG(23)	SD(23)	Gouge	Gouge	Gouge	Gouge	Gouge	Gouge	Gouge
XRF									
SiO_2	65.22	0.09	60.01	64.82	64.99	65.16	62.93	65.04	64.98
Al_2O_3	17.29	0.08	17.73	17.43	17.38	17.44	18.79	17.27	17.33
FeO*	3.98	0.05	6.00	4.03	4.08	3.99	3.88	4.03	4.05
MgO	1.86	0.05	3.19	1.98	1.95	1.88	1.94	1.91	1.84
CaO	4.75	0.03	6.25	4.89	4.86	4.82	5.73	4.80	4.80
Na_2O	4.63	0.08	4.29	4.62	4.48	4.48	4.78	4.66	4.69
K_2O	1.43	0.02	1.23	1.38	1.39	1.39	1.14	1.43	1.42
TiO_2	0.62	0.01	0.96	0.63	0.66	0.62	0.62	0.62	0.61
P_2O_5	0.15	0.02	0.23	0.15	0.13	0.14	0.13	0.17	0.20
MnO	0.07	0.00	0.11	0.07	0.07	0.07	0.07	0.07	0.07
Total	100.00	0.00	100.0	100.0	100.0	100.0	100.0	100.0	100.0
ICP-MS									
Ba	340	18	284	300	328	341	307	337	314
Be	1.3	0.1	1.4	1.2	1.6	1.5	1.4	1.1	1.0
Cd	0.10	0.09	0.06	0.05	0.04	0.03	0.2	0.04	0.03
Ce	24.6	1.1	31.0	22.5	24.6	24.7	20.1	25.5	22.9
Co	11.5	0.7	20.6	11.4	11.8	11.8	12.9	10.3	10.2
Cr	8.9	1.1	19.2	9.1	10.7	9.6	11.4	7.9	7.8
Cs	1.6	0.1	0.9	1.5	1.6	1.5	1.6	1.4	1.4
Cu	33.3	3.2	48.3	31.2	35.8	29.1	37.1	29.2	28.2
Ga	19.5	0.8	20.2	18.5	19.1	19.9	22.0	18.0	18.0
La	12.7	0.4	15.0	11.8	12.6	12.6	10.7	12.9	12.2
Li	24.7	2.0	16.6	24.2	25.6	26.0	28.8	21.2	17.7
Nb	5.4	1.3	10.0	5.5	3.1	4.4	5.4	3.7	6.7
Ni	8.3	1.0	25.6	7.9	9.2	8.4	10.6	9.0	7.6
P	616	41	1030	558	630	613	590	600	565
Pb	7.63	0.62	5.23	7.24	7.32	6.60	10.8	7.60	6.04
Rb	33.7	1.1	23.0	32.4	33.0	33.2	27.2	32.0	32.7
Sb	0.2	0.1	0.1	0.1	0.2	0.2	0.2	0.2	0.2
Sc	9.4	0.6	16.7	9.1	9.6	9.8	10.3	8.2	8.2
Sr	471	11	514	490	465	472	602	464	455
Th	2.75	0.24	2.29	2.26	2.63	2.21	2.00	2.40	2.61
U	1.05	0.11	0.86	0.7	1.05	0.62	0.63	0.85	1.09
V	75	6	137	74	78	80	83	47	49
Y	11.8	0.7	18.0	9.7	11.7	10.8	9.9	11.3	12.3
Zn	60	3	79	62	68	61	70	55	56
ED-XRF									
Zr	119	19	161	132	95	90	NA	123	123

Note: X-ray fluorescence (XRF) analyses are reported in weight percent. FeO* indicates all iron reported as FeO. Inductively coupled plasma–mass spectrometric (ICP-MS) analyses and energy-dispersive XRF (ED-XRF) analyses are reported in parts per million (ppm). Eruption dates were estimated by projecting location of sample back to the vent at the relevant linear eruption rate (Pallister et al., 2008). All analyses were conducted at Washington State University.

1999; Tuffen et al., 2008). However, there is no compelling reason to call on such a process for the 2004–2008 Mount St. Helens earthquakes because the dacite magma within the conduit had already solidified at the depth of the shallow seismogenic zone. Because the cataclasites of the fault zone would have required extensive rock fracture and shearing in their generation, it seems logical that the process was "noisy," i.e., it was capable of producing earthquakes. However, can we relate the observed eruption seismicity at Mount St. Helens to structures and fabrics in the spines?

With few exceptions, volcano-tectonic earthquakes with coda magnitudes (M_d) >0 were restricted to the initial "vent clearing" phase of the eruption (23 September through 5 October 2004); they are attributed to fracturing of more competent rock below the crater floor (Moran et al., 2008; Thelen et al., 2008). In contrast, the subsequent dome-forming phase of the eruption was instead accompanied by more than a million small ($M_d < 2.0$) repetitive low-frequency "drumbeat" events, along with occasional larger earthquakes and very long period events (Lehto et al., 2010; Moran et al., 2008; Thelen et al., 2008; Waite et al., 2008). In addition, many more microearthquakes (as used here, earthquakes with $M_d < 0$) occurred but were too small to be recorded except at near-vent seismic stations (Moran et al., 2008; Thelen et al., 2008). Two contrasting models for the source of the drumbeat earthquakes have been proposed: stick-slip at the conduit margins and associated periodic motion of the spine-plug above a compressible magma column (Harrington and Brodsky, 2007; Iverson, 2008; Iverson et al., 2006) or gas-driven oscillation of cracks in the crater floor (Waite et al., 2008). In the following section, we evaluate these models in the context of our field observations, moment magnitudes, and seismic moments.

Stick-Slip Models

Let us assume that each earthquake records a slip event in the fault zone surrounding the conduit. Neglecting aseismic creep for the moment, the average slip would then equal the measured linear extrusion rate divided by the number of earthquakes per unit time. For a well-constrained interval in December 2004 when spine 4 was being extruded and drumbeat earthquakes were repeating at ~60 s intervals (1440 earthquakes per day) and the average linear extrusion rate was ~6 m/d (Major et al., 2008), the result is ~4 mm/earthquake. Yet, the relationship between drumbeat spacing and event size was complex and varied widely during the month despite continued extrusion (e.g., on 16 December 2004,

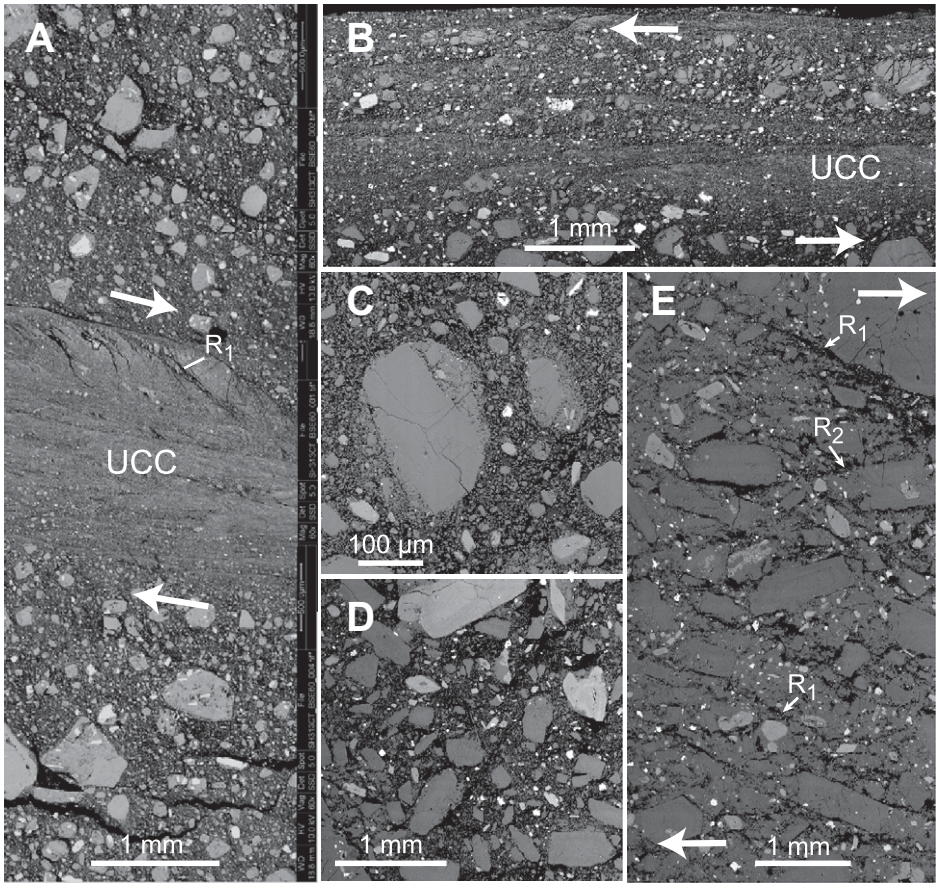

Figure 10. Backscattered scanning electron microscope (SEM) images of samples from the Mount St. Helens conduit-margin fault zone exposed on spine 4. (A) Gouge sample dredged from fault core, showing ultracataclasite layer (UCC) with micro-Riedel shears (R). (B) Gouge sample from surface of fault core collected in place and showing development of ultracataclasite layers and shear fragmentation of grains. (C) Higher-magnification image of gouge sample from 3 cm distance into spine showing milled phenocryst fragments with adhering cataclastic matrix and surrounded by ultracataclasite matrix with an average grain size of <10 µm. (D) Matrix of cataclastic breccia from 20 cm distance into the spine. Matrix grain size ranges from ~10 µm to 100 µm. (E) Sheared dacite from 1 to 2 m into the damage zone of the spine, showing intact phenocrysts, concentration of deformation in the groundmass, and development of conjugate Riedel shears (synthetic R_1 shears are inclined to the right in the image, and antithetic R_2 shears are inclined to the left in the image). Arrows indicate sense of shear in A, B, and E. Sections B–E were collected from a measured section perpendicular to the spine surface.

the average M_d was ~1.5 and event spacing was ~90 s; on 23 December 2004, the average M_d was ~0.5 and spacing was ~40 s; Moran et al., 2008). In addition, from textures indicative of grain flow and microscopic shearing in spine 4, we know that a significant fraction of the motion during this interval must have been effectively aseismic. Therefore, we consider 4 mm to be a maximum average displacement for the typical drumbeat earthquake during the extrusion of spine 4.

We considered calculating expected slip-patch dimensions for the drumbeat earthquakes by substituting a range of measured magnitudes into empirically determined equations for tectonic faults that relate local magnitude (M_L), moment magnitude (Mw), seismic moment (Mo), and shear modulus (µ) to slip-patch dimensions (Dowrick and Rhoades, 2004; Hanks and Kanamori, 1979; Kanamori, 1977). However, the lack of a simple relationship between measured M_d and local magnitude (M_L) for the drumbeat earthquakes at Mount St. Helens (Qamar et al., 2008) prevents determination of Mw and use of this method. Instead, we used the relationship between corner frequency and seismic moment as determined by Harrington and Brodsky (2007) from empirical Green's function pulses for more than 100 earthquakes recorded at near-vent stations in 2005 at Mount St. Helens. This analysis yields an average stress drop of ~0.5 MPa (5×10^5 Nm^2) and Mo ~2×10^{10} Nm for the *typical* drumbeat earthquake (i.e., the midpoint of the cluster in fig. 3 *in* Harrington and Brodsky, 2007). Using this average seismic moment, we calculate the maximum expected slip-patch area by substituting the 4 mm average displacement for December 2004 into the seismic moment equation of Hanks and Kanamori (1979):

$$\mathrm{Mo} = \mu LWD \text{ or } \mathrm{Mo} = \mu A_S D,$$

in which L = subsurface rupture length (in m), W = subsurface rupture width (in m), the seismically determined slip-patch area (A_S) = $L \times W$ (in m^2), D = mean displacement (m) over the rupture area, and µ = modulus of rigidity (or shear modulus, in Nm^{-2}). A rectangular slip patch is used here rather than a more conventional circular slip-patch area for convenience in comparison to the rectangular areas of Riedel shear planes and to the piston-like geometry of the spines.

A µ value of ~3.0×10^{10} Nm^{-2} (30 GPa) is typically used for tectonic earthquake studies and corresponds to the experimentally determined shear modulus for felsic igneous and metamorphic rocks (Birch, 1966). In contrast, a lower µ value of ~5×10^9 Nm^2 was calculated from the 5×10^5 Nm^2 stress drop of Harrington and Brodsky (2007) and a 0.0001 ratio of stress drop to shear modulus (Kanamori, 1977). Petrology and brittle textures tell us that the Mount St. Helens dacite had completely solidified to dacite rock prior to formation of the bounding fault zone. However, the conduit rock was hot, and much of the deformation took place within reduced-strength cataclastic rocks of the fault zone. Consequently, we regard the µ value of ~5×10^9 Nm^2 to be a reasonable average value, and we calculate a maximum average slip-patch area for a typical drumbeat earthquake of ~10^3 m^2 (equivalent to a rectangular area of ~30 m × ~30 m) assuming D = 4 mm.

For evaluating seismic moment in terms of fault-plane geometry and observed seismic magnitudes, we can define a geological slip-patch area (A_G) based on field data, and then compare this value to the expected A_S calculated previously. Using this approach, we evaluated stick-slip models for the two candidate slip patches observed in the field: principal shear zones and Riedel shears. Given the geologic uncertainties involved in using an average D value, in using stress drop data from a relatively small

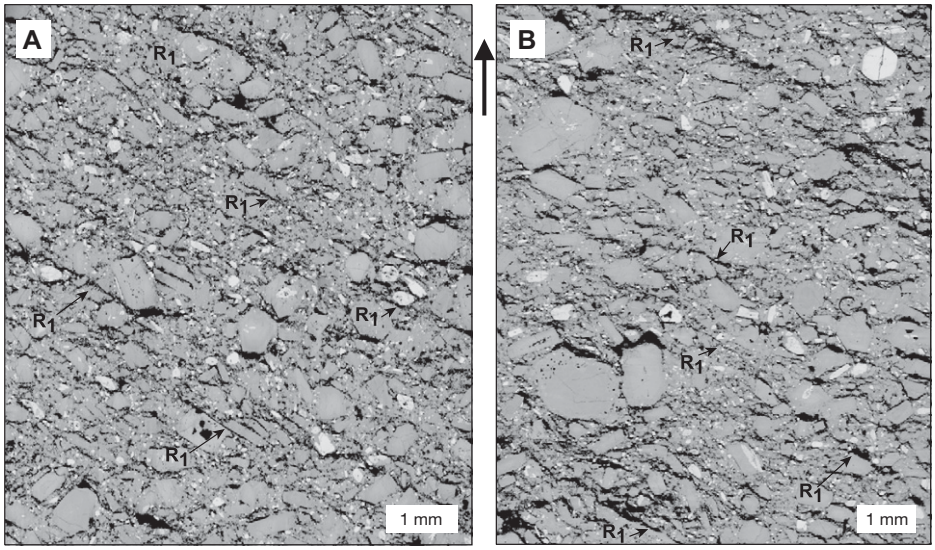

Figure 11. Photomicrographs of polished sections from oriented samples of sheared dacite at 1–2 m into the damage zone of spine 4. The paired figures highlight the pervasive and through-going nature of the fracturing, which results in a porosity of 8%–9% (as measured in these images). These textures show that porosity and permeability are generated prior to gouge formation. As in Figure 10E, deformation is concentrated in the groundmass and results in prominent synthetic Riedel shears (R_1; inclined to the right in the images). (A) Section cut perpendicular to transport direction. (B) Section cut on a plane parallel to the transport direction of the spine. Arrow indicates the direction toward the outer margin of the spine in both images. Consequently, and as seen in outcrop, the prominent Riedel shears in A dip back toward the vent and are consistent with the overall shear couple for extrusion, whereas the less prominent Riedel shears in B suggest additional circumferential shear along the conduit margin.

number of 2005 Mount St. Helens earthquakes as representative, and in using a moment value for a typical drumbeat, we consider only order-of-magnitude differences in A_S and A_G to be meaningful.

(1) Distributed Riedel shear model. In this model, we assumed that drumbeat faulting was the result of distributed shearing along the hundreds of thousands of megascopic Riedel shears within the dacite of the conduit-margin damage zone. Riedel shears of the damage zone are typically <2 m in dimension in transport-parallel cross sections, and they occur as self-similar families of fractures bounded by through-going principal shear zones (e.g., Figs. 7 and 8). As previously noted, transport-normal dimensions are more difficult to determine, as multiple individual Riedel shears typically merge into through-going fractures. However, the larger of these fractures typically extend for a few tens of meters (Fig. 9A). We conclude that the individual megascopic Riedel shear patches seen in outcrops have A_G areas of ≤100 m^2, i.e., an order of magnitude less than the seismically determined average slip-patch area calculated previously (~10^3 m^2), and therefore are insufficient to produce the typical drumbeat earthquake. However, these are of sufficient area to produce $M_d < 0$ microearthquakes, as observed on close-in seismic stations throughout the 2004–2008 eruption (Moran et al., 2008; Thelen et al., 2008). Alternatively, we consider the possibility that dozens of the Riedel structures in the same area could fail together in domino fashion and thereby constitute a larger composite slip patch. Although more complex, such a failure mode is permissive from the field data.

(2) Principal shear zones and SPASM. In the Seismogenic Plug of Ascending, Solidifying Magma (SPASM) model of Iverson (2008), a cylindrical fault surrounds a plug of solidified dacite. Stick-slip cycles of motion and drumbeat earthquakes are modeled as a consequence of periodic slip of the plug margins, accompanied by vertical displacement of the plug above compressible conduit magma at greater depth. Such a model is supported by the presence of asperities on the surfaces of the principal shear zones, which imply that these surfaces periodically stuck, built up strain, and were released (Fig. 5B).

To test if field and petrologic data support the SPASM model, we used the same procedure as described above, i.e., comparing A_S to A_G. The first case we considered was the same as in the distributed Riedel shear model and posed the question: Is there observational evidence of slip patches with areas on the order of ~10^3 m on the principal shear zones? If the fault motion was incremental and divergent in orientation at this scale, we would expect a "patchwork" of relatively small (e.g., ~30 m × ~30 m) principal shear zones with divergent slip directions covering the spine surfaces. Such features were not evident in our studies of spine 4 or from helicopter-borne observations during the eruption. Instead, we observed grooves on the principal shear zone–covered spine surfaces that were parallel for hundreds of meters (Fig. 1), indicative of unidirectional motion. The question that logically follows is: What field evidence would be anticipated if the motion were incremental and unidirectional? If the times between increments of movement were long enough, we might find depositional markers analogous to the "bathtub rings" produced by nightly wetting cycles at the vent (Vallance et al., 2008). However, except for millimeter-scale asperities along slickensides, we did not find any structural indicators that established incremental motion on the principal shear zones. Consequently, the field data do not favor incremental and divergent motion, but they are permissive (but not conclusive) for incremental and unidirectional motion of the dacite plug along the principal shear zones.

We can also consider full-plug slip by "unwrapping" a section of the cylinder to a rectangular slip patch with width (W) equal to the circumference of the conduit and length (L) equal to the height above the solidification zone. Based on field observations of an ~120 m vent diameter (Vallance et al., 2008), we set W to a value of ~380 m. If we then assume that the full height of the solidified section of the conduit moved as a plug, we can set L = 500–1000 m based on the petrologic estimations of the solidification zone depth, yielding A_G = ~2 × 10^5 m^2 to ~4 × 10^5 m^2, i.e., two orders of magnitude greater than the average value of A_S calculated previously. In order to have $A_G = A_S$, D would need to be reduced to ~0.01–~0.03 mm, i.e., two orders of magnitude less than the 4 mm maximum displacement per drumbeat calculated previously. Such small displacements would produce only microearthquakes. In summary, our field data do not support coherent full-plug stick slip to produce the drumbeat earthquakes, and they are permissive (but not conclusive) with respect to generation of the drumbeat earthquakes by distributed and incremental movement along the conduit-bounding principal shear zones.

(3) Rock mechanics model. A rock mechanics study of the Mount St. Helens spines (Kennedy

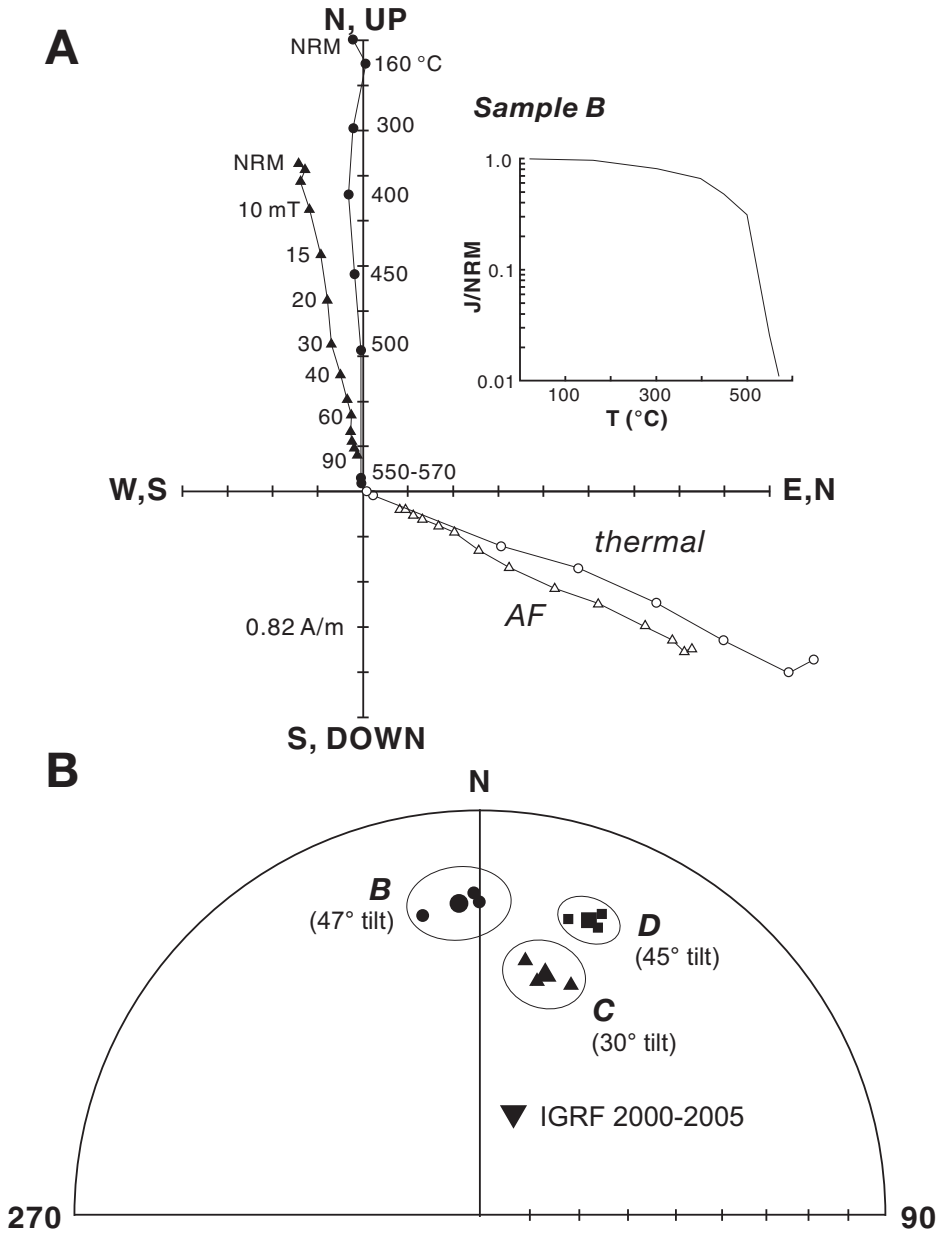

Figure 12. (A) Orthogonal plot of alternating field (AF; triangles) and thermal demagnetization (circles) vector end points for two specimens of cataclasite. Filled symbols are projected onto the horizontal plane, and unfilled symbols are projected onto the vertical plane. Inset shows a plot of the normalized intensity versus demagnetization temperature for a thermally treated specimen. NRM refers to the natural remanent magnetization. (B) Equal-area plot of paleomagnetic directions and sample mean directions with their 95% confidence limits. Inverted triangle (IGRF) indicates the modeled present-day geomagnetic field direction at Mount St. Helens. The tilts of spine 4 were calculated between this reference direction and the sample mean directions.

et al., 2009) provides additional insight into the origin of the conduit-margin fault zone and its possible relationship to seismic activity. These authors showed that gouge produced experimentally at room temperature from the spine dacite is remarkably similar to that produced at ~730 °C and to that in the natural gouge samples. These results confirm our conclusions based on petrologic and paleomagnetic data that the Mount St. Helens dacite solidified at relatively high temperatures in the subsurface prior to brittle failure. They also show that at displacement rates of ~10^{-4} cm s^{-1}, displacements of up to 2.5 mm produce micro–fault zones with thicknesses of up to 0.2 mm. Kennedy et al. (2009) used these data to calculate theoretical strain rates and gouge thicknesses. Assuming localized shear on multiple surfaces in the 1–3-m-thick gouge and linear extrusion rates of ~3–6 m d^{-1}, they calculated strain rates of ~5×10^{-2} s^{-1} to 5×10^{-1} s^{-1} for each slip event. These are close to the strain rates anticipated for coseismic slip and a permissive cause for the drumbeat seismicity. Conversely, distributing the displacements across the 1–3-m-thick gouge zone reduces the strain rates to ~10^{-4} s^{-1} to 10^{-5} s^{-1}, i.e., values indicative of fault creep and too slow to account for the drumbeat seismicity. However, in extrapolating the experimentally determined microfault growth rates to the Mount St. Helens conduit dimensions, Kennedy et al. (2009) calculated that gouge thicknesses of 0.8–5 mm and average strike lengths of 98–190 m per drumbeat earthquake would produce the observed 1–3 m thickness of gouge. These dimensions are within the range of observed principal shear zones and, like our work, offer permissive but nonunique or conclusive support for stick-slip generation of the earthquakes on these structures.

A Resonating Steam-Filled Crack Model (Waite et al., 2008)

This is an elegant seismological model based on data from a temporary broadband seismic network that was deployed at Mount St. Helens crater during the summer of 2005. This modeled solution for the Long-Period (LP) drumbeat earthquakes calls for a nondestructive volumetric source, which is best fit by a gently dipping NNW-striking, steam-filled crack located at shallow levels (200 ± 100 m) under the spines in the southern part of the crater. The best-fit elevation of the modeled crack is at ~2000 m above sea level (asl), i.e., at or near the level of the base of the 1980 crater-fill deposits (Fig. 14). Resonance of the crack as a result of periodic release of steam pressure is modeled as the source of the drumbeat earthquakes.

According to this model, deformation within the margins of the spines must have been effectively aseismic (Matoza et al., 2009). Our structural and textural data do not directly bear on this model, except to the extent that they document structures within the conduit-bounding fault zone that are responsible for the micro-earthquakes. However, other field and monitoring data do bear more directly on the resonating crack model. The linkage of drumbeat earthquakes and infrasound emissions (Matoza et al., 2009) is one of the most compelling arguments

TABLE 2. ELECTRON MICROPROBE ANALYSES OF Fe-Ti OXIDES, TEMPERATURES, AND OXYGEN FUGACITIES FOR A SAMPLE OF SHEARED DACITE FROM SPINE 4

Sample*	SiO_2	TiO_2	Al_2O_3	Cr_2O_3	FeO	MnO	MgO	Na_2O	NiO	P_2O_5	Total
P60622Be-1 MT	0.04	17.50	0.95	0.05	73.00	0.33	1.16	0.01	0.09	0.00	93.13
SD (5)	0.02	0.77	0.03	0.02	0.75	0.02	0.04	0.01	0.13	0.00	0.45
P60622Be-1 IL	0.00	47.25	0.10	0.02	48.10	0.52	2.11	0.01	0.08	0.00	98.18
SD(5)	0.00	0.18	0.01	0.01	0.47	0.02	0.08	0.01	0.11	0.00	0.45
P60622Be-2 MT	0.06	16.12	0.97	0.01	75.26	0.37	1.24	0.01	0.11	0.02	94.17
SD(8)	0.02	0.30	0.03	0.01	0.64	0.02	0.02	0.01	0.14	0.01	0.45
P60622Be-2 IL	0.00	46.94	0.10	0.01	48.47	0.46	2.08	0.01	0.03	0.01	98.11
SD(8)	0.01	0.21	0.01	0.01	0.18	0.02	0.03	0.01	0.09	0.01	0.39
P60622Be-3 MT	0.09	13.00	1.01	0.01	77.14	0.40	1.04	0.01	0.10	0.00	92.81
SD(4)	0.03	1.49	0.09	0.01	2.31	0.02	0.10	0.01	0.14	0.00	1.15
P60622Be-3 IL	0.02	46.33	0.09	0.01	48.12	0.53	2.05	0.00	0.05	0.01	97.21
SD(5)	0.02	0.25	0.01	0.01	0.29	0.01	0.05	0.01	0.04	0.01	0.30
P60622Be-3 MT	1.63	13.79	1.06	0.03	73.58	0.44	1.15	0.03	0.03	0.07	91.81
SD(4)	0.60	0.36	0.04	0.02	1.38	0.03	0.05	0.00	0.06	0.05	1.45
P60622Be-4 IL	0.15	45.44	0.12	0.00	47.66	0.59	2.01	0.01	0.00	0.02	95.99
SD(6)	0.04	0.52	0.01	0.00	0.50	0.02	0.02	0.01	0.00	0.02	0.42
P60622Be-5 MT	0.00	11.05	1.72	0.04	79.89	0.30	1.27	0.01	0.11	0.01	94.40
SD(10)	0.00	0.64	0.04	0.02	0.61	0.02	0.05	0.01	0.15	0.01	0.44
P60622B-5e IL	0.00	45.10	0.13	0.01	49.95	0.41	2.40	0.01	0.00	0.01	98.01
SD(7)	0.00	1.00	0.03	0.01	0.66	0.04	0.18	0.01	0.00	0.01	0.37

Sample	Spots	Description	Avg. T (°C)			Log f_{O_2}		
P60622Be-1	10	Exsolved titanomagnetite (8 µm spots)	933	±	3	−11.70	±	0.03
P60622Be-2	16	Unexsolved pair in large fragment	906	±	2	−12.02	±	0.03
P60622Be-3	9	Unexsolved pair in large fragment	859	±	14	−12.65	±	0.19
P60622Be-4	9	Unexsolved pair in large fragment	897	±	8	−12.05	±	0.12
P60622Be-5	17	Exsolved matrix grains (20 µm spots)	865	±	8	−12.07	±	0.13

Note: All analyses were conducted at U.S. Geological Survey laboratories in Denver, Colorado, using a JEOL Superprobe. ZAF corrections for atomic number effects (Z), absorption (A), and fluorescence (F) utilized natural mineral standards, an accelerating voltage of 15 kV, and a beam current of ~2.0×10^{-8} A. Electron beam spot size was ~1 µm unless otherwise indicated. SD refers to standard deviation for the number of analyses spots in parentheses. Oxide abundances reported as weight percent.

*Touching titanomagnetite (MT) and ilmenite (IL) grain pairs are indicated by suffix numbers 1–4. Pair 5 represents the average analyses of nontouching small grains in the groundmass of the sample.

for associating the earthquakes with gas emissions. Yet, the location of the modeled crack and emissions in the southern part of the crater is difficult to reconcile with the scarcity of observed gas emissions in this area during the eruption. Matoza et al. (2009) acknowledged this fact, but argued that such emissions were dissipated into the porous ≥1980 crater-fill rocks.

Recent experimental simulations of seismic signals from wet and dry volcanic rock showed that acoustic events occurring under dry conditions follow the expected scaling of moment and corner frequencies for standard brittle failure, whereas those produced under wet conditions do not (Harrington and Benson, 2011). This relation and scaling dissimilarities between field observations led these authors to conclude that the hybrids at Mount St. Helens did not occur as the result of a fluid process.

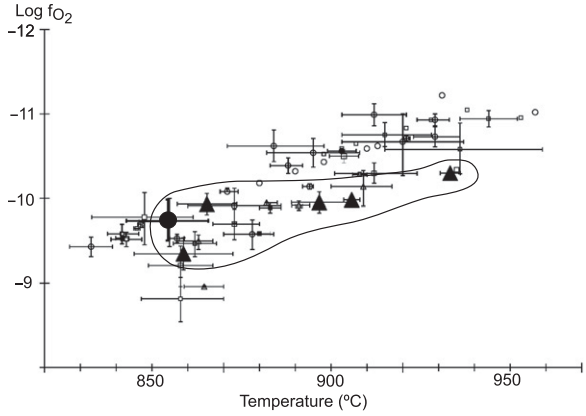

Figure 13. Thermobarometric results from oxide analyses of 2006 gouge sample P-60622-Be (black triangles enclosed in field) compared to results from dacite lava samples from the 2004–2008 data set of Pallister et al. (2008) (open circles). Black circle gives original temperature for the 2004 magma. Other data points are for zoned oxides from 2004 to 2008 spines; the wide ranges in apparent temperature and oxygen fugacities for these oxides are attributed to latent heating resulting from extensive groundmass crystallization (Pallister et al., 2008). Error bars are based ±1 standard deviation of determinations for multiple grain pairs in individual samples as detailed in Pallister et al. (2008).

Constraints from Gas Emissions, Nondestructive Seismic Sources, and Linking Stick-Slip and Resonating Crack Models

It could be argued that the low levels of volcanic gas emissions (in particular of SO_2 and CO_2) during the 2004–2008 eruption favor stick-slip mechanisms over fluid movement or resonance mechanisms for the longer-period drumbeat earthquakes. However, these arguments neglect the significant amount of water vapor that was liberated during magma ascent and solidification. Gerlach et al. (2008) estimated that closed-system ascent of the dacite magma from the magma reservoir at 5 km to solidification depths of 0.5–1 km would have reduced H_2O in the matrix melt from ~4.4 wt% to 1.2 wt% H_2O, while the separated fluid phase ($X_{H_2O} = 0.98$) expanded from 11 vol% at 5 km to 60–80 vol% gas in the solidification interval. This is more than enough fluid to produce a compressible magma capable of modulating stick-slip cycles of movement (Iverson, 2008) or to cause long-period earthquakes as some of this steam escaped through fractures in crater-floor rocks (Waite et al., 2008).

Steam emissions were observed from active fumaroles along the northern margin of the spines throughout the eruptions (Fig. 15). On

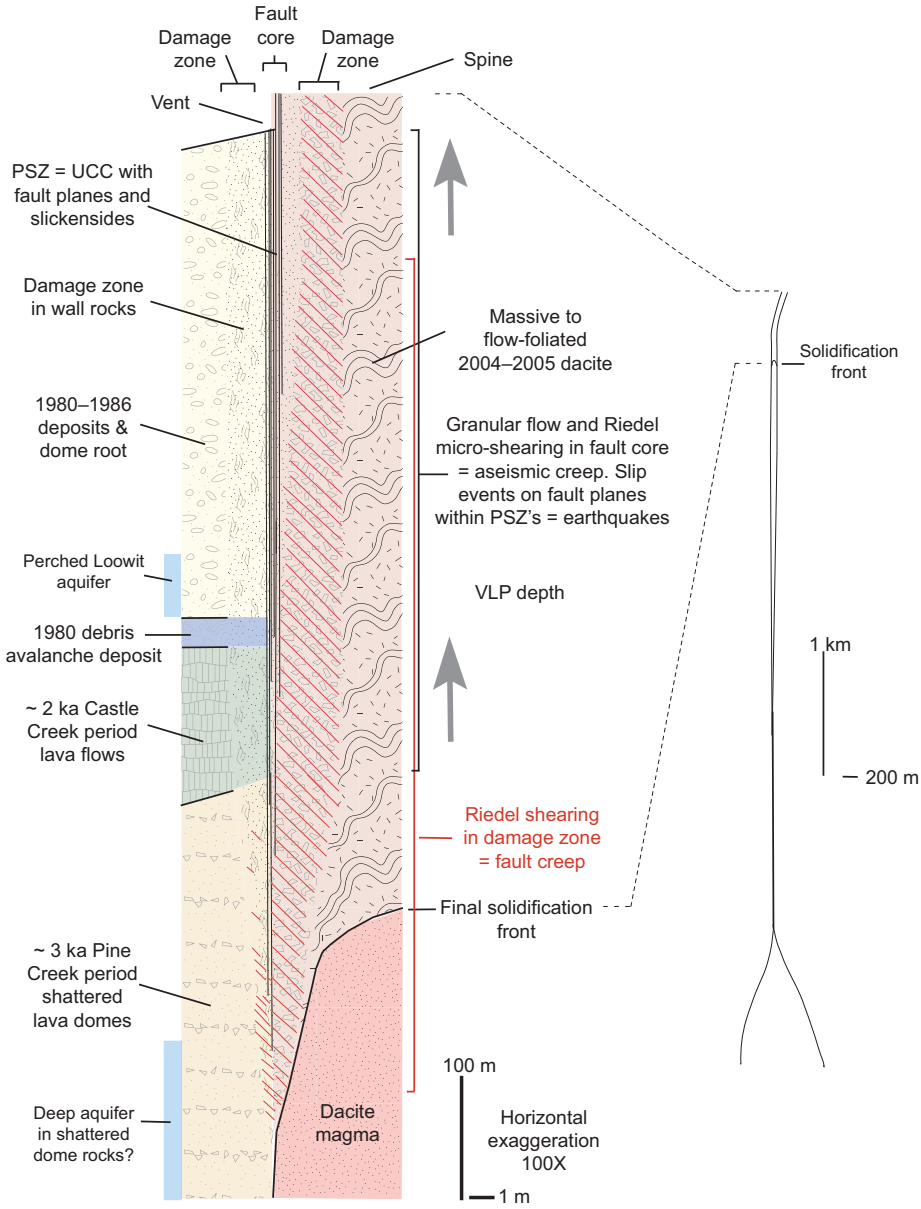

Figure 14. Model cross section of the Mount St. Helens conduit-spine system showing progressive development of the marginal fault zone. Only half of the conduit is shown, and the inclination of the upper part of the conduit (see inset diagram) and root of the 1980–1986 dome are omitted. Positions of subsurface units (Pine Creek period lava domes, and Castle Creek period lava; Crandell, 1987) as well as the 1980–1986 deposits and the Loowit aquifer are projected on the basis of geologic mapping by the first author. Two candidate stick-slip earthquake and aseismic creep zones are also indicated by number (see text). UCC—ultracataclasite; PSZ—principal shear zone; VLP—very long period earthquakes.

14 January 2005, one of the authors (Pallister) photographed steam and minor ash jetting from one of these fumaroles, which at the time was emitting a roaring noise. These fumarole areas were also the sources for the only explosive events during the eruption: the ash emissions of 1, 3, 4, and 5 October 2004, 16 January 2005, and 8 March 2005 (Scott et al., 2008). The north edge of the spines lies above the southward flexure of the conduit, a tensional environment that enables easy egress of gases to the surface. Similar ash and gas plumes emanated from the equivalent position where curved spines at the Soufriere Hills lava dome detached from adjacent wall rocks and emerged from the vent (Sparks, 2000). In terms of geologic observations, these spine-margin steam vents are an obvious alternative source for infrasound emissions; however, their location at the northern margin of the spines, rather than in the southern part of the crater where the hypocenters are located (Thelen et al., 2008), is problematic.

In any case, the maintenance of "self-similar" sources for thousands of drumbeat earthquakes as families of multiplets (Thelen et al., 2008) over the long-duration eruption is interpreted by us as requiring an unusual geologic situation in which a nondestructive earthquake source must have been maintained. Volume changes of ~1000 m^3 are called for in the resonating steam-filled crack model, equivalent to as much as 5 cm movement per earthquake cycle for a 150 m × 150 m × 10 m crack (Waite et al., 2008). From a geologic point of view, one would expect degradation of a crack within the rocks at shallow levels below the Mount St. Helens crater floor after only a few cycles of such movement. However, in the case of stick-slip models, continued delivery of fresh rock to the seismogenic zone by the conveyor-belt–like replenishment process envisioned in Figure 14 would have produced self-similar conduit-margin fault structures as seen in the spine outcrops.

Given the high vertical permeability of the conduit-bounding fault rocks (Gaunt et al., 2011), it is likely that gas was transported upward around the full circumference of the spines. One possibility to help reconcile the stick-slip and resonating crack models is that stick-slip events along the conduit boundary fault not only produced microearthquakes (and possibly drumbeats), but they also opened pathways for gas transport. The resulting gas pulses could have reached the surface both through fumaroles along the northern tensional margin of the spines as well as exciting resonance of cracks below the crater floor.

SUMMARY

We document conclusive geologic and textural evidence for a brittle fault zone forming shallow levels of the Mount St. Helens conduit and surrounding the extruding dacite plug—a fault that formed during the extensively monitored 2004–2008 spine-forming eruption. The conduit-boundary fault has structural and textural features that are similar to those seen at shallow levels of seismogenic tectonic faults, including a characteristic damage zone and fault core profile. Deformation originated by Riedel shearing in the damage zone, but the majority of fault motion was partitioned into a series of thin, but areally extensive, ultracataclasite layers (principal shear zones) within the fault core. We present a cross-sectional model for the upper

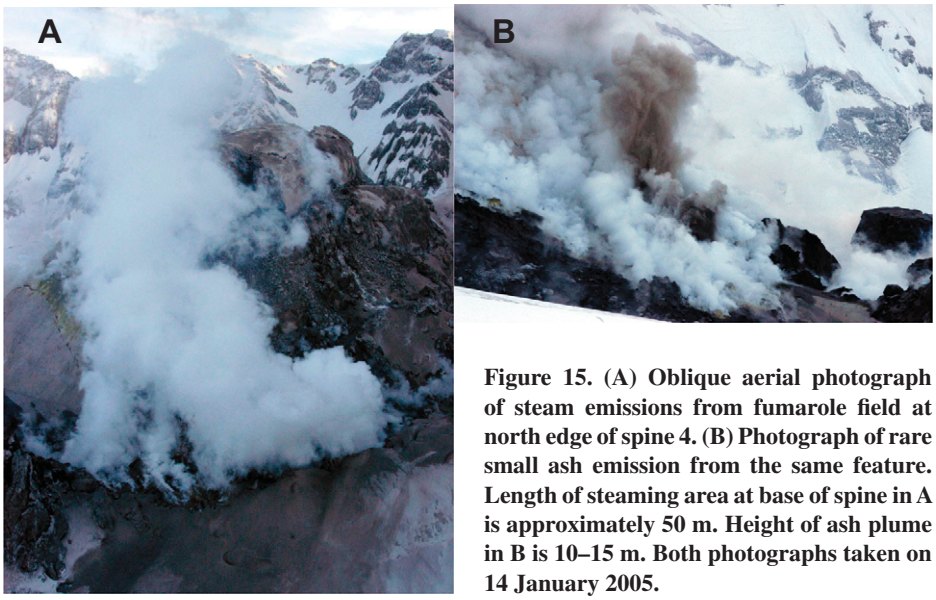

Figure 15. (A) Oblique aerial photograph of steam emissions from fumarole field at north edge of spine 4. (B) Photograph of rare small ash emission from the same feature. Length of steaming area at base of spine in A is approximately 50 m. Height of ash plume in B is 10–15 m. Both photographs taken on 14 January 2005.

kilometer of the conduit in which the bounding fault zone developed continuously in conveyor-belt fashion as dacite magma was first solidified by decompression crystallization and then underwent brittle deformation in a sustained shear couple between the ascending plug and wall rocks. Relatively low volatile content of the 2004–2008 dacite and relatively slow ascent prevented explosive fragmentation and enabled development of the spines.

Our analysis of seismic moments indicates that Riedel shearing in the damage zone (as well as creep by granular flow in gouge of the fault core) was mainly aseismic with respect to most stations in the monitoring network. Field data are permissive but not conclusive with respect to incremental movement along the conduit-bounding principal shear zones to produce the drumbeat earthquakes. In short, our geologic field and textural data indicate fault creep and generation of microearthquakes within the conduit-boundary fault zone, and they offer permissive but not conclusive evidence for generation of the drumbeat earthquakes.

In spite of the lack of conclusive evidence concerning stick-slip or crack resonance models for the Mount St. Helens drumbeat earthquakes, our geologic data and the resulting cross section of the conduit-bounding fault zone, combined with the detailed monitoring, observational, and petrologic data from the eruption (Sherrod et al., 2008) provide an unusually rich framework for detailed studies of the deformation that accompanies magma ascent. Such studies are under way at Mount St. Helens (e.g., Friedlander et al., 2010; Gaunt et al., 2011; Kennedy et al., 2009; Smith et al., 2011) and at other volcanoes (e.g., Holland et al., 2011; Neuberg et al., 2006). They provide an unusual opportunity to relate geophysical monitoring data to magma ascent processes—an important step in improving process-oriented eruption forecasting. As an example, within the U.S. Geological Survey–U.S. Agency for International Development Volcano Disaster Assistance Program (VDAP), we have successfully interpreted the occurrence of drumbeat earthquakes as precursors for degassed dome extrusion at multiple volcanoes in Latin America and Indonesia.

ACKNOWLEDGMENTS

The authors acknowledge the contributions of numerous USGS and university colleagues who participated in the response to and subsequent study of the 2004–2008 eruption of Mount St. Helens. Discussions and field work with many of these colleagues were instrumental in developing the concepts presented here. We also appreciate constructive manuscript reviews by Lori Kennedy, Michael Ort, John Ewert, and an anonymous reviewer.

REFERENCES CITED

Ahlgren, S.G., 2001, The nucleation and evolution of Riedel shear zones as deformation bands in porous sandstone: Journal of Structural Geology, v. 23, p. 1203–1214, doi:10.1016/S0191-8141(00)00183-8.

Andersen, D.H., and Lindsay, J.R., 1988, Internally consistent solution models for Fe-Mg-Mn-Ti oxides: The American Mineralogist, v. 73, p. 714–726.

Bacon, C.R., and Hirschmann, M.M., 1988, Mg/Mn partitioning as a test for equilibrium between coexisting Fe-Ti oxides: The American Mineralogist, v. 73, p. 57–61.

Ben-Zion, Y., and Sammis, C., 2003, Characterization of fault zones: Pure and Applied Geophysics, v. 160, p. 677–715, doi:10.1007/PL00012554.

Birch, F., 1966, Compressibility; elastic constants, *in* Clark, S.P., Jr., ed., Handbook of Physical Constants: Geological Society of America Memoir 97, p. 97–173.

Blundy, J., Cashman, K., and Humphreys, M., 2006, Magma heating by decompression-driven crystallization beneath andesite volcanoes: Nature, v. 443, p. 76–80, doi:10.1038/nature05100.

Blundy, J., Cashman, K.V., and Berlo, K., 2008, Evolving magma storage conditions beneath Mount St. Helens inferred from chemical variations in melt inclusions from the 1980–1986 and current (2004–2006) eruptions, *in* Sherrod, D.R., Scott, W.E., and Stauffer, P.H., eds., A Volcano Rekindled: The Renewed Eruptions of Mount St. Helens, 2004–2006: U.S. Geological Survey Professional Paper 1750, p. 755–790.

Bogoyavlenskaya G.E., and Kirsanov I.T., 1981, Twenty five years of volcanic activity of Bezymianny: Volcanologiya i Seysmologiyal, v. 1981, Issue 2, p. 3–13 (in Russian).

Brace, W.F., Paulding, B.W., and Scholz, C., 1966, Dilatancy in the fracture of crystalline rocks: Journal of Geophysical Research, v. 71, p. 3939–3953, doi:10.1029/JZ071i016p03939.

Caine, J.S., Evans, J.P., and Forster, C.B., 1996, Fault zone architecture and permeability structure: Geology, v. 24, p. 1025–1028, doi:10.1130/0091-7613(1996)024<1025:FZAAPS>2.3.CO;2.

Cashman, K., 2004, Volatile controls on magma ascent and eruption, *in* Sparks, R.S.J., and Hawkesworth, C.J., eds., The State of the Planet: Frontiers and Challenges in Geophysics: International Union of Geodesy and Geophysics Geophysical Monograph 150, v. 19, p. 109–124.

Cashman, K., Thornber, C.R., and Pallister, J.S., 2008, From dome to dust: Shallow crystallization and fragmentation of conduit magma during the 2004–2006 dome extrusion of Mount St. Helens, Washington, *in* Sherrod, D.R., Scott, W.E., and Stauffer, P.H., eds., A Volcano Rekindled: The Renewed Eruptions of Mount St. Helens, 2004–2006: U.S. Geological Survey Professional Paper 1750, p. 387–413.

Chester, F.M., and Logan, J.M., 1987, Composite planar fabric of gouge from the Punchbowl fault, California: Journal of Structural Geology, v. 9, p. 621–634, doi:10.1016/0191-8141(87)90147-7.

Chouet, B.A., 1996, Long-period volcano seismicity: Its source and use in eruption forecasting, Nature, v. 380, p. 309–316.

Clynne, M.A., Calvert, A.T., Wolfe, E.W., Evarts, R.C., Fleck, R.J., and Lanphere, M.A., 2008, The Pleistocene eruptive history of Mount St. Helens, Washington: From 300,000 to 12,800 years before present, *in* Sherrod, D.R., Scott, W.E., and Stauffer, P.H., eds., A Volcano Rekindled: The Renewed Eruptions of Mount St. Helens, 2004–2006: U.S. Geological Survey Professional Paper 1750, p. 593–627.

Crandell, D., 1987, Deposits of Pre-1980 Pyroclastic Flows and Lahars from Mount St. Helens Volcano, Washington: U.S. Geological Survey Professional Paper 1444, 91 p.

Doblas, M., 1998, Slickenside kinematic indicators: Tectonophysics, v. 295, p. 187–197, doi:10.1016/S0040-1951(98)00120-6.

Dowrick, D.W., and Rhoades, D.A., 2004, Relations between earthquake magnitude and rupture dimensions. How regionally variable are they?: Bulletin of the Seismological Society of America, v. 94, p. 776–788, doi:10.1785/0120030151.

Fisher, R.A., 1953, Dispersion on a sphere: Proceedings of the Royal Society of London, ser. A, v. 217, p. 295–305, doi:10.1098/rspa.1953.0064.

Friedlander, B., Kennedy, L.A., Russell, J.K., and Pallister, J.S., 2010, Mechanisms of strain localization within the 2004–2008 Mt. St. Helens lava domes: The role of effusion rate?: Eos (Transactions, American Geophysical Union), Abstract V54B–08, presented at 2010 Fall Meeting, AGU, San Francisco, Calif., 13–17 Dec.

Gaunt, H.E., Meredith, P.G., Sammonds, P.R., Smith, R., and Kilburn, C., 2011, Factors controlling permeability and fluid flow within the 2004–2008 Mount St. Helens lava dome complex: Eos (Transactions, American Geophysical Union), Abstract V23F–2621, presented at 2011 Fall Meeting, AGU, San Francisco, Calif., 5–9 Dec.

Gerlach, T.M., McGee, K.A., and Doukas, M., 2008, Emission rates of CO_2, SO_2, and H_2S, scrubbing, and preeruption excess volatiles at Mount St. Helens, 2004–2005, *in* Sherrod, D.R., Scott, W.E., and Stauffer, P.H., eds., A Volcano Rekindled: The Renewed Erup-

tions of Mount St. Helens, 2004–2006: U.S. Geological Survey Professional Paper 1750, p. 543–572.

Goto, A., 1999, A new model for volcanic earthquake at Unzen Volcano: Melt rupture model: Geophysical Research Letters, v. 26, p. 2541–2544, doi:10.1029/1999GL900569.

Hanks, T.C., and Kanamori, H., 1979, A moment magnitude scale: Journal of Geophysical Research, v. 84, p. 2348–2350, doi:10.1029/JB084iB05p02348.

Harrington, R.M., and Benson, P.M., 2011, Analysis of laboratory simulations of volcanic hybrid earthquakes using empirical Green's functions: Journal of Geophysical Research, v. 116, p. B11303, doi:10.1029/2011JB008373.

Harrington, R.M., and Brodsky, E.E., 2007, Volcanic hybrid earthquakes that are brittle-failure events: Geophysical Research Letters, v. 34, L06308, doi:10.1029/2006GL028714.

Harrington, R.M., and Kwiatek, G., 2011, Seismically radiated energy per unit area 758 remains constant for families of volcanic hybrid earthquakes associated with the 2004–2008 759 Mount St. Helens dome building eruption, Abstract S53B-2283 presented at the Fall Meeting, AGU, San Francisco, Calif., 5–9 Dec.

Herriott, T.M., Sherrod, D.R., Pallister, J.S., and Vallance, J.W., 2008, Photogeologic maps of the 2004–2005 Mount St. Helens eruption, *in* Sherrod, D.R., Scott, W.E., and Stauffer, P.H., eds., A Volcano Rekindled: The Renewed Eruptions of Mount St. Helens, 2004–2006: U.S. Geological Survey Professional Paper 1750, p. 209–224.

Holland, A.S.P., Watson, I.M., Phillips, J.C., Caricchi, L., and Dalton, M.P., 2011, Degassing processes during lava dome growth: Insights from Santiguito lava dome, Guatemala: Journal of Volcanology and Geothermal Research, v. 202, p. 153–166, doi:10.1016/j.jvolgeores.2011.02.004.

Iverson, R.M., 2008, Dynamics of seismogenic volcanic extrusion resisted by a solid surface plug, Mount St. Helens, 2004–2005, *in* Sherrod, D.R., Scott, W.E., and Stauffer, P.H., eds., A Volcano Rekindled: The Renewed Eruptions of Mount St. Helens, 2004–2006: U.S. Geological Survey Professional Paper 1750, p. 425–460.

Iverson, R.M., and 13 others, 2006, Dynamics of seismogenic volcanic extrusion at Mount St. Helens in 2004–2005: Nature, v. 444, p. 439–443, doi:10.1038/nature05322.

Kanamori, H., 1977, The energy release in great earthquakes: Journal of Geophysical Research, v. 82, p. 2981–2987, doi:10.1029/JB082i020p02981.

Kennedy, L.A., and Russell, J.K., 2011, Cataclastic production of volcanic ash at Mount Saint Helens: Physics and Chemistry of the Earth, v. 45–46, p. 40–49.

Kennedy, L.A., Russell, J.K., and Nelles, E., 2009, Origins of Mount St. Helens cataclasites: Experimental insights: The American Mineralogist, v. 94, p. 995–1004, doi:10.2138/am.2009.3129.

Kerr, R.A., 2003, High-tech fingers on Earth's erratic pulse: Science, v. 299, p. 2016–2020, doi:10.1126/science.299.5615.2016.

Kirschvink, J.L., 1980, The least-squares line and plane and analysis of paleomagnetic data: Geophysical Journal of the Royal Astronomical Society, v. 62, p. 699–718, doi:10.1111/j.1365-246X.1980.tb02601.x.

Lacroix, A., 1904, La Montagne Pelé et ses Eruptions: Paris, Masson, 662 p.

Lehto, H.L., Roman, D.C., and Moran, S.C., 2010, Temporal changes in stress preceding the 2004–2008 eruption of Mount St. Helens, Washington: Journal of Volcanology and Geothermal Research, v. 198, p. 129–142, doi:10.1016/j.jvolgeores.2010.08.015.

Major, J.J., Kingsbury, C.G., Poland, M.P., LaHusen, R.G., and Dzurisin, D., 2008, Extrusion rate of the Mount St. Helens lava dome estimated from terrestrial imagery, November 2004–December 2005, *in* Sherrod, D.R., Scott, W.E., and Stauffer, P.H., eds., A Volcano Rekindled: The Renewed Eruptions of Mount St. Helens, 2004–2006: U.S. Geological Survey Professional Paper 1750, p. 237–256.

Matoza, R.S., Garcés, M.A., Chouet, B.A., D'Auria, L.D., Hedlin, M.A.H., De Groot-Hedlin, C., and Waite, G.P., 2009, The source of infrasound associated with long-period events at Mount St. Helens: Journal of Geophysical Research, v. 114, B04305, doi:10.1029/2008JB006128.

McChesney, P.J., Couchman, M., Moran, S.C., Lockhart, A.B., Swinford, K., and LaHusen, R.G., 2008, Seismic monitoring deployments and instrument development (seismic spider) at Mount St. Helens 2004–2005, *in* Sherrod, D.R., Scott, W.E., and Stauffer, P.H., eds., A Volcano Rekindled: The Renewed Eruptions of Mount St. Helens, 2004–2006: U.S. Geological Survey Professional Paper 1750, p. 129–144.

McNutt, S.R., 1996, Seismic monitoring and eruption forecasting of volcanoes: A review of the state-of-the-art and case histories, *in* Scarpa, T., ed., Monitoring and Mitigation of Volcano Hazards: Berlin, Germany, Springer-Verlag, p. 99–196.

McNutt, S.R., 2005, Volcano seismology: Annual Review of Earth and Planetary Sciences, v. 33, p. 461–491, doi:10.1146/annurev.earth.33.092203.122459.

Mimatsu, M., 1995, Showa-Shinzan Diary: Hokkaido, Japan, Sobetsu Town Office, Expanded Reprint, 179 p.

Moore, D.E., and Byerlee, J.D., 1991, Comparative geometry of the San Andreas fault, California, and laboratory fault zones: Geological Society of America Bulletin, v. 103, p. 762–774, doi:10.1130/0016-7606(1991)103<0762:CGOTSA>2.3.CO;2.

Moore, P.L., Iverson, N.R., and Iverson, R.M., 2008, Frictional properties of the 2004–2005 Mount St. Helens gouge, *in* Sherrod, D.R., Scott, W.E., and Stauffer, P.H., eds., A Volcano Rekindled: The Renewed Eruptions of Mount St. Helens, 2004–2006: U.S. Geological Survey Professional Paper 1750, p. 415–423.

Moran, S.C., Malone, S., Qamar, A.I., Thelen, W., Wright, A.K., and Caplan-Auerbach, J., 2008, Seismicity associated with the renewed dome-building eruption of Mount St. Helens, 2004–2005, *in* Sherrod, D.R., Scott, W.E., and Stauffer, P.H., eds., A Volcano Rekindled: The Renewed Eruption of Mount St. Helens, 2004–2006: U.S. Geological Survey Professional Paper 1750, p. 27–60.

Neuberg, J.W., Tuffen, H., Collier, H., Green, D., Powell, T., and Dingwell, D.B., 2006, The trigger mechanism of low-frequency earthquakes on Montserrat: Journal of Volcanology and Geothermal Research, v. 153, p. 37–50, doi:10.1016/j.jvolgeores.2005.08.008.

Pallister, J.S., Thornber, C.R., Cashman, K.V., Clynne, M.A., Lowers, H.A., Mandeville, C., Brownfield, I.K., and Meeker, G.P., 2008, Petrology of the 2004–2005 Mount St. Helens lava dome—Implications for magmatic plumbing and eruption triggering, *in* Sherrod, D.R., Scott, W.E., and Stauffer, P.H., eds., A Volcano Rekindled: The Renewed Eruptions of Mount St. Helens, 2004–2006: U.S. Geological Survey Professional Paper 1750, p. 647–702.

Qamar, A.I., Malone, S.D., Moran, S.C., Steele, W.P., and Thelen, W.A., 2008, Near-real-time information products for Mount St. Helens—Tracking the ongoing eruption, *in* Sherrod, D.R., Scott, W.E., and Stauffer, P.H., eds., A Volcano Rekindled: The Renewed Eruptions of Mount St. Helens, 2004–2006: U.S. Geological Survey Professional Paper 1750, p. 61–70.

Riedel, W., 1929, Zür mechanik geologischer brucherscheinungen: Zentralblatt für Mineralogie, Geologie und Paleontologie, v. B, p. 354–368.

Rowe, M.C., Thornber, C.R., and Kent, A.J.R., 2008, Identification and evolution of the juvenile component in 2004–2005 Mount St. Helens ash, *in* Sherrod, D.R., Scott, W.E., and Stauffer, P.H., eds., A Volcano Rekindled: The Renewed Eruptions of Mount St. Helens, 2004–2006: U.S. Geological Survey Professional Paper 1750, p. 629–646.

Rutherford, M.J., 2008, Magma ascent rates: Reviews in Mineralogy and Geochemistry, v. 69, p. 241–271, doi:10.2138/rmg.2008.69.7.

Rutherford, M.J., and Devine, J.D., III, 2008, Magmatic conditions and processes in the storage zone of the 2004–06 Mount St. Helens eruptions, *in* Sherrod, D.R., Scott, W.E., and Stauffer, P.H., eds., A Volcano Rekindled: The Renewed Eruptions of Mount St. Helens, 2004–2006: U.S. Geological Survey Professional Paper 1750, p. 703–725.

Sammonds, P.R., Smith, R., Tuffen, H., and Meredith, P.G., 2010, Mechanical evolution of the 2004–2008 Mount St. Helens lava dome mechanics with time and temperature: Eos (Transactions, American Geophysical Union), Abstract V33c-2391, presented at 2010 Fall Meeting, AGU, San Francisco, Calif., 13–17 Dec.

Schneider, D., Vallance, J., Wessels, R.L., Logan, M., and Ramsey, M.S., 2008, Use of thermal infrared imaging for monitoring renewed dome growth at Mount St. Helens, 2004, *in* Sherrod, D.R., Scott, W.E., and Stauffer, P.H., eds., A Volcano Rekindled: The Renewed Eruptions of Mount St. Helens, 2004–2006: U.S. Geological Survey Professional Paper 1750, p. 347–359.

Scholz, C.H., 1987, Wear and gouge formation in brittle faulting: Geology, v. 15, p. 493–495, doi:10.1130/0091-7613(1987)15<493:WAGFIB>2.0.CO;2.

Scott, W.E., Sherrod, D.R., and Gardner, C.A., 2008, Overview of 2004 to 2006, and continuing, eruption of Mount St. Helens, Washington, *in* Sherrod, D.R., Scott, W.E., and Stauffer, P.H., eds., A Volcano Rekindled: The Renewed Eruptions of Mount St. Helens, 2004–2006: U.S. Geological Survey Professional Paper 1750, p. 3–22.

Sherrod, D.R., Scott, W.E., and Stauffer, P.H., eds., 2008, A Volcano Rekindled: The Renewed Eruption of Mount St. Helens, 2004–2006: U.S. Geological Survey Professional Paper 1750, 856 p.

Sibson, R.H., 1977, Fault rocks and fault mechanisms: Journal of the Geological Society of London, v. 133, p. 191–213, doi:10.1144/gsjgs.133.3.0191.

Skempton, A.W., 1966, Some observations on tectonic shear zones: Proceedings of the 1st International Congress on Rock Mechanics: Lisbon, International Society for Rock Mechanics, p. 329–335.

Smith, R., Sammonds, P.R., Tuffen, H., and Meredith, P.G., 2009, The 2004–2008 Mount St. Helens lava dome: An experimental study of the influence of time and temperature on mechanical behaviour and earthquakes: Eos (Transactions, American Geophysical Union), v. 90, Abstract V12A–02.

Smith, R., Sammonds, P.R., Tuffen, H., and Meredith, P.G., 2011, Evolution of the mechanics of the 2004–2008 Mt. St. Helens lava dome with time and temperature: Earth and Planetary Science Letters, v. 307, p. 191–200, doi:10.1016/j.epsl.2011.04.044.

Sparks, R.S.J., 2000, Control on the emplacement of the andesite lava dome of the Soufriere Hills volcano, Montserrat, by degassing-induced crystallization: Terra Nova, v. 12, p. 14–20, doi:10.1046/j.1365-3121.2000.00267.x.

Stormer, J.C., 1983, The effects of recalculation on estimates of temperature and oxygen fugacity from analyses of multi-component iron-titanium oxides: The American Mineralogist, v. 68, p. 586–594.

Swanson, D.A., and Holcomb, R.T., 1990, Regularities in growth of the Mount St. Helens dacite dome, *in* Fink, J.H., ed., Lava Flows and Domes: Berlin, Springer, International Association of Volcanology and Chemistry of the Earth's Interior Proceedings in Volcanology, p. 3–25.

Tchalenko, J.S., 1970, Similarities between shear zones of different magnitudes: Geological Society of America Bulletin, v. 81, p. 1625–1640, doi:10.1130/0016-7606(1970)81[1625:SBSZOD]2.0.CO;2.

Thelen, W., Crosson, R.S., and Creager, K.C., 2008, Absolute and relative locations for earthquakes at Mount St. Helens using continuous data: Implications for magmatic processes, *in* Sherrod, D.R., Scott, W.E., and Stauffer, P.H., eds., A Volcano Rekindled: The Renewed Eruptions of Mount St. Helens, 2004–2006: U.S. Geological Survey Professional Paper 1750, p. 71–95.

Tuffen, H., Smith, R., and Sammonds, P.R., 2008, Evidence for seismogenic fracture of silicic magma: Nature, v. 453, p. 511–514, doi:10.1038/nature06989.

Vallance, J.W., Schneider, D.J., and Schilling, S.P., 2008, Growth of the 2004–2006 lava-dome complex at Mount St. Helens, Washington, *in* Sherrod, D.R., Scott, W.E., and Stauffer, P.H., eds., A Volcano Rekindled: The Renewed Eruptions of Mount St. Helens, 2004–2006: U.S. Geological Survey Professional Paper 1750, p. 169–208.

Waite, G.P., Chouet, B.A., and Dawson, P.B., 2008, Eruption dynamics at Mount St. Helens imaged from broadband seismic waveforms: Interaction of the shallow magmatic and hydrothermal systems: Journal of Geophysical Research, v. 113, B02305, doi:10.1029/2007JB005259.

Walder, J.S., Schilling, S.P., Vallance, J.W., and LaHusen, R.G., 2008, Effects of lava-dome growth on the Crater Glacier of Mount St. Helens, *in* Sherrod, D.R., Scott, W.E., and Stauffer, P.H., eds., A Volcano Rekindled: The Renewed Eruptions of Mount St. Helens, 2004–2006: U.S. Geological Survey Professional Paper 1750, p. 257–276.

Watts, R.B., Heard, R.A., Sparks, R.S.J., and Young, S.R., 2002, Growth patterns and emplacement of the andesitic lava dome at Soufrière Hills Volcano, Montserrat, *in* Druitt, T.H., and Kokelaar, B.P., eds., The Eruption of Soufrière Hills Volcano, Montserrat, from 1995 to 1999: Geological Society of London Memoir 21, p. 115–152.

White, R.A., 1996, Precursory deep long-period earthquakes at Mount Pinatubo; spatio-temporal link to a basalt trigger, *in* Newhall, C.G., and Punongbayan, R.S., eds., Fire and Mud: Eruptions and lahars of Mount Pinatubo, Philippines: Philippine Institute of Volcanology and Seismicity (Quezon City) and University of Washington Press (Seattle), p. 307–328.

White, R. A., Miller, A.D., Lynch, L., and Power, J., 1998, Observations of hybrid seismic events at Soufriere Hills Volcano, Montserrat: July 1995 to September 1996: Geophysical Research Letters, v. 25, p. 3657–3660, doi:10.1029/98GL02427.

Science Editor: Nancy Riggs
Associate Editor: Michael Ort

Manuscript Received 24 April 2012
Revised Manuscript Received 5 August 2012
Manuscript Accepted 17 August 2012

Printed in the USA